NASA Contractor Report 178184

(NASA-CR-178184) SPACE-BASED LASER-DRIVEN MHD GENERATOR: FEASIBILITY STUDY Final Report (Information and Control Systems, Inc.) 52 p CSCL 10C

N87-11837

Unclas
G3/20 44917

SPACE-BASED LASER-DRIVEN MHD GENERATOR:
FEASIBILITY STUDY

S. H. Choi

INFORMATION & CONTROL SYSTEMS, INC.
Hampton, Virginia

Purchase Order L-28161B
October 1986

National Aeronautics and
Space Administration

Langley Research Center
Hampton, Virginia 23665

SPACE-BASED LASER-DRIVEN MHD GENERATOR: FEASIBILITY STUDY

S. H. Choi
Information & Control Systems, Inc.

SUMMARY

The feasibility of a laser-driven MHD generator, as a candidate receiver for a space-based laser power transmission system, was investigated.

An extensive literature search of research on MHD generators and laser-produced plasmas was carried out. The MHD generators were tabulated according to characteristics such as the energy source, working fluid, generator type, flow rate, temperature, electrical conductivity, power density, generator dimension, efficiency, magnetic field strength, seed material, type of cycle, and operating mode. Laser-produced plasma and laser plasma interactions were tabulated with respect to plasma temperature, laser type and energy, plasma conductivity, absorption of laser radiation, flow velocity, carrier gas, and seed material.

On the basis of reasonable parameters obtained in the literature search, a model of the laser-driven MHD generator was developed with the assumptions of a steady, turbulent, two-dimensional flow. The assumptions used in this study were based on the continuous and steady generation of plasmas by the exposure of the continuous wave laser beam thus inducing a steady back pressure that enables the medium to flow steadily. The model considered here took the turbulent nature of plasmas into account in the two-dimensional geometry of the generator. For these conditions with the plasma parameters defining the thermal conductivity, viscosity, electrical conductivity for the plasma flow, a generator efficiency of 53.5 percent was calculated. If turbulent effects and nonequilibrium ionization are taken into account, the efficiency is 43.2 percent.

The study shows that the laser-driven MHD system has potential as a laser power receiver for space applications because of its high energy conversion efficiency, high energy density and relatively simple mechanism as compared to other energy conversion cycles.

LIST OF FIGURES

LIST OF TABLES

LIST OF SYMBOLS

a - degree of ionization

A - generator cross-sectional area, m^2

$\overline{A}$ - Van Driest constant

Ar - Argon

$\overline{b}$ - Mei and Squire constant

B - magnetic field

C - specific heat, J/kg·K

C_f - friction coefficient

C_s - Cesium

D - plasma diameter, m

e - electronic charge, C

Ec - Eckert number, $\overline{U}^2/C_p\, T_w$

g_c - gravity, m/s^2

h - Planck constant

H - height, m

Ha - Hartmann number, $LB\left(\frac{\sigma_e}{\mu}\right)^{\frac{1}{2}}$

He - Helium

j - current, A

J - non-dimensional current

k - thermal conductivity, W/mk

K - ratio of load to open circuit voltages

$\overline{k}$ - von Karman constant

L - characteristic length, m

n_e - electron density, m^{-3}

N - ratio of molecular thermal conduction to radiation for a gas

LIST OF SYMBOLS (CONTINUED)

N_B	- density of Argon or helium
P	- power density output, W/m^3
P_{in}	- power density input, W/m^3
P_r	- Prandtl number
Pr_t	- turbulent Prandtl number
q'_r	- radiation heat flux, W/m^2
q'_x	- radiation heat flux in the x-direction, W/m^2
q'_y	- radiation heat flux in the y-direction, W/m^2
$\dot{q}''_{w1,2}$	- heat flux through the boundary, W/m^2
Q_x	- radiation heat flux ratio in the x-direction
Q_y	- radiation heat flux ratio in the y-direction
Q(T)	- collisional cross section
Re	- Reynolds number
Re_t	- turbulent Reynolds number
r_n	- hydraulic radius
t	- scaled time
t'	- time, s
T'	- temperture, K
U'	- velocity, m/s
$\overline{U}$	- average velocity, m/s
U_c	- centerline velocity, m/s
V	- velocity ratio, $U'_z/\overline{U}$
W	- width, m
x'	- x' direction length in the coordinate, m

X - scaled length in the x' direction

y' - y' direction length in the coordinate, m

Y - scaled length in the y' direction

z' - z' direction length in the coordinate, m

Z - scaled length in the z' direction

$\overline{Z}$ - turbulent distance

Greek:

α - thermal diffusity, m^2/s

α_τ - turbulent thermal diffusivity, m^2/s

β - ratio of the electron mean-free-path to the Larmor radius

ε_o - permitivity of free space

ρ - density, kg/m^3

ρ_d - Debye radius

κ - Boltzmann constant, J/K

$\overline{\kappa}$ - absorption coefficient

θ - scaled temperature

τ_o - optical thickness, m

σ - electrical conductivity, S/m

σ_{eff} - effective electrical conductivity, S/m

ν - kinematic viscosity, m^2/s

ν_τ - turbulent kinematic viscosity, m^2/s

γ' - shear stess, Pa

γ - the lowering of the ionization potential by the Debye cloud

η - scaled distance, or efficiency

LIST OF SYMBOLS (CONCLUDED)

Greek (continued):

ξ - plasma turbulence factor

μ - electron mobility

ζ - a parameter defined by $H_a^2/(Re_t \cdot n)$ in the Function F_1

Δ - characteristic focal dimension defined by $\Delta = 1\sqrt{(4.8/D)^2 + (\pi/L)^2}$

Subscripts:

B - combination of the He and Ar

C - centerline

C_s - cesium

d - Debye

M - Magnetic field

t - turbulent

w - wall

W_1 - wall 1

W_2 - wall 2

x - x direction

y - y direction

ABBREVIATIONS

UT	- United Technology
GE	- General Electric Company
AVCO	- AVCO - Everett Research Lab
BMI	- Battelle Memorial Institute
UTSI	- University of Tennessee Space Institute
SU	- Stanford University
ARGAS-I	- MHD Generator name, by Eindhoven
MIT	- Massachussetts Institute of Technology
JPL	- Jet Propulsion Lab
ANL	- Argonne National Lab
AI	- Atomic International

INTRODUCTION

The advantages of using a laser to transmit power in space is based on three features of the laser:

1. The laser beam can be transmitted over long distances without appreciable attenuation or divergence,

2. The laser provides a high source intensity at the receiver,

3. The laser does not require physical contact between energy source and power generator.

While the laser appears to be an advantageous means of transmitting energy in space, the means of beam generation and beam conversion to a more useful form of energy (i.e., electricity or propulsion) are not well defined. Converter systems, in particular, must meet the requirements of high conversion efficiency at a high energy density while remaining small, light weight and simple. One converter system which may meet the requirements is the laser-driven MHD generator which is shown in Figure 1. The plasma is produced by focusing the laser beam into the plasma production chamber. At sufficiently high intensity, breakdown will occur in the gas medium producing a plasma. Once the plasma is established, it will absorb the laser radiation which will heat the plasma. Although the laser driven MHD generator is an efficient candidate energy conversion system for space abplication, the absorption of transmitted beam energy by the participating medium in the plasma production chamber becomes the key factor in determining the generator efficiency. With the proper plasma conditions such as laser peak power, gas pressure, gas species, focal volume density, and plasma temperature, absorption of the laser beam can reach 80% with Nd long pulse laser light of approximately 10^{18} W/m^2 and 65% with CO_2 long pulse laser light of roughly 10^{17} W/m^2 (Ref. 1). Figure 2 shows the estimated efficiencies of a laser-driven MHD generator subsystem.

This preliminary study of the laser driven MHD generator includes a literature survey and a development of a simplified theoretical model for the system. The literature survey was conducted to establish realistic parameters, such as temperature and density, for laser produced plasmas and also to determine those design parameters of MHD channels which are affected by the plasma conditions such as plasma temperature and density. Both plasma and liquid metal MHD generators were included in the literature survey.

The primary purpose of the study was to identify certain characteristics of existing MHD generator systems so that these characteristics could be used in the development of a prototype design for a laser driven MHD generator. System characteristics such as the energy source, generator type, working fluid, working fluid flow, temperature, electrical conductivity, power density, generator dimension, magnetic field, cycle features, seed material and mode of operation were considered.

1. Plasma MHD

The characteristics of plasma MHD generator systems are given in Table I. The systems can be divided into four groups: 1) shock-driven, 2) arc, 3) combustion (including coal burning), and 4) explosive-driven (including rocket and detonation). The primary difference between these systems and the laser-driven MHD generator is the method of plasma production, although some differences in the flow of the plasma through the channel occurs. The shock or explosive driven MHD generators, for example, are characterized by quasi-adiabatic wave propagation through the channel and a rapid decay of the plasma after the wave has passed. In the laser-driven MHD generator, on the other hand, the plasma flow will be exposed to the laser radiation (so long as the critical charge density which produces optical reflection is not reached), and heating of the plasma throughout the channel will occur. The flow in the laser-driven MHD channel is expected to be an unsteady, turbulent flow with a heat source. The power density in a MHD generator depends on the average channel velocity, the magnetic field intensity, and the electrical conductivity.

2. Liquid Metal MHD

The characteristics of liquid metal MHD systems are given in Table II. The conceptual and experimental works done so far are directly applicable to the laser-driven liquid metal MHD system, since the configuration of the conventional liquid metal MHD systems is the same except for the laser beam receiver. The laser energy is supplied through the optical system in which the beam energy is converted into the driving power of the liquid metal (two-phase flow).

Liquid metal MHD systems usually deal with low temperature energy sources. Hence, they do not have the hardware related problems, such as melting, that may take place in the plasma MHD generator. The corrosion and the separation of gas from liquid (in the case of two-phase flow) are the main problems to be solved.

Table III gives the alkali metal parameters such as the ionization potential, the percent ionization, and the absorption length at 2500K and 10333 Pa(1 atm).

3. Laser Plasma Interaction

The plasma is produced by a gas breakdown after threshold irradiance has been achieved. This gas breakdown process proceeds in the following steps: (1) the production of the initial ionization, and (2) the subsequent cascade by which the ioniztion grows and the shock wave propagates, and dissipates.

After the initial ionization is produced, its growth becomes the dominant process. Following a small amount of ionization, free electrons absorb photon energy by inverse bremsstrahlung. When an electron has gained enough energy, it can ionize an additional atom in a collision. The electron is then replaced by two electrons with lower energy in the free electron continuum. Both electrons then absorb energy by inverse bremsstrahlung, and cascading of the ionization occurs. This cascade process, fed by the absorption of laser light in the inverse bremsstrahlung process, is the mechanism which produces the growth of the ionization.

Breakdown threshold of the gas, as a function of intensity, depends on the focal volume. As the focal volume becomes smaller, losses, either by diffusion of the electrons out of the focal region or by radiation, limit the build up and increase the threshold. The cascade process proceeds more rapidly, for a given irradiance, with a larger focal volume. To maintain the growth of the cascade for a stable plasma within the focal volume, the following criteria should be met:

(1) large focal volume

(2) high beam flux density (over 7×10^{18} W/m^2)

(3) continuous wave beam flux (CW laser)

(4) high gas density

(5) low boundary effects.

The power output requirements of the laser as an energy source for a laser-driven MHD generator can be chosen by the focal volume of the plasma chamber, gas pressure, gas species, MHD channel geometry, etc.

Breakdown characteristics are shown in Figures 2, 4, 5 and 6. The gas breakdown threshold is a function of the gas pressure and focal volume. The breakdown threshold exhibits a linear relationship with the peak irradiance, but this relationship also depends on the species and pressures of the gas. For argon gas at pressures of 1 atm, 2 atm, and 38.2 atm (lines C, D, and E shown in Fig. 5), the breakdown has a different behavior at 1 atm than at 3 atm. At constant pressure of a participating gas, the absorption of laser beam energy depends on the peak input power. Figure 6 shows the aspect of beam transmission through the air at a pressure of 746 torr when a Ruby laser pulse is focused through a 0.0206 m focal length lens. Breakdown is also a function of the incident radiation wavelength and the density of the medium (see Fig. 7). The absorption of the laser beam occurs at high pressure (or density), and the time required for breakdown threshold must be short due to fast energy accumulations. At this state after breakdown, the dominant energy transfer mechanism (on a microscopic time scale) is inverse bremsstrahlung rather than conduction or diffusion.

In Table IV, the relevant laser-plasma interaction parameters obtained from the literature survey are tabulated in order of the laser sources, target medium, breakdown laser power, plasma temperature, plasma electron density, dimension of the plasma, and propagation velocity.

The laser considered in the tabulation of Table IV are the 10.6 μm CO_2, Ruby pulse, and Nd-glass lasers. The media were air, argon, helium, nitrogen, deuterium, and plastic pellet at various pressures.

A SIMPLIFIED MHD MODEL CALCULATION

The MHD system selected here for study is a plasma MHD generator. The model of a selected MHD generator is set-up and simplified with the assumptions that the system is under operation.

1. MHD Channel Model

The channel schematic selected for study is depicted in Figures 1 and 8 and consists of a hydrodynamically, thermally stable turbulent flow of an electrically conducting and radiating gas, between electrode plates with a uniform, constant magnetic field applied in the positive x-direction. The channel side walls and the electrode walls have either a constant heat flux or a constant temperature. The physical properties of the gas are constant and the gas is in local thermodynamic equilibrium. The gas has a refractive index of unity, and scattering effects are negligible.

For the calculations, the geometrical dimensions and the boundary conditions for the channel must be considered. Table V shows the parameters which are necessary for calculating the MHD generator performance. The initial and boundary conditions for the governing equations are determined from solutions to the equations for the laser-plasma interaction. For simulation purposes, the initial and boundary conditions can be obtained from experimental data.

2. Energy Balance

The thermal energy equation in this study considers the fully developed, turbulent flow of an electrically conducting and radiating gas in a rectangular duct, where viscous dissipation and Joule heating effects are considered; but axial components of conduction and radiation are neglected (since their contributions to the velocity and temperature fields are small compared to those of the other terms in the equation). Thus the energy equation may be written in the following form:

$$\rho c \frac{\partial T'}{\partial t'} + \rho c \, U'_y \frac{\partial T'}{\partial y'} + \rho c \, U'_x \frac{\partial T'}{\partial x'} + \rho c \, U'_z \frac{\partial T'}{\partial z'}$$

$$= \frac{\partial}{\partial y'} \left[k\left(1 + \frac{\alpha_t}{\alpha}\right) \frac{\partial T'}{\partial y'} \right] + \frac{\partial}{\partial x'} \left[k\left(1 + \frac{\alpha_t}{\alpha}\right) \frac{\partial T'}{\partial x'} \right]$$

$$+ \mu\left(1 + \frac{\nu_t}{\nu}\right) \left(\frac{\partial U'_z}{\partial y'}\right)^2 + \mu\left(1 + \frac{\nu_t}{\nu}\right) \left(\frac{\partial U'_z}{\partial x'}\right)^2 + \frac{j^2}{\sigma_e} - \frac{\partial q'_r}{\partial y'} - \frac{\partial q'_r}{\partial x'} \tag{1}$$

ORIGINAL PAGE IS
OF POOR QUALITY

The first two terms on the right hand side (RHS) represent the net thermal energy transport due to molecular flow and turbulent transport with α_t denoting the turbulent diffusivity of heat. The rest of the terms on the RHS are (in order shown): the molecular and turbulent viscous dissipation with ν_t being the turbulent viscous dissipation of momentum, Joule heating with σ_{eff} denoting the gas electrical conductivity, and divergence of the radiative flux. The turbulent transport quantities are assumed to vary across the channel. The boundary conditions for the above equations are described by two possible cases:

1) Constant wall temperature

$$T'(y=0) = T'(y=\pm H/2) = T'_{w_1}$$
$$T'(x=0) = T'(x=\pm \frac{W}{2}) = T'_{w_2} \tag{2a}$$

2) Constant heat flux

$$\frac{\partial T'}{\partial y'}(y=0) = \frac{\partial T'}{\partial y'}(y=\pm \frac{H}{2}) = -\frac{\dot{q}''_{w_1}}{k}$$
$$\frac{\partial T'}{\partial x'}(x=0) = \frac{\partial T'}{\partial x'}(x=\pm \frac{W}{2}) = -\frac{\dot{q}''_{w_2}}{k} \tag{2b}$$

where $\dot{q}''_{w_1}$ and $\dot{q}''_{w_2}$ are the heat fluxes through the boundary.

The initial conditions depend on the entry plasma characteristics. These can be defined by experimental measurement and treated as input variables. Initially these conditions, listed in the bottom of Table II, were selected from the literature for the study. The boundary conditions in the z-direction totally depend on the initial conditions and on the time dependence of temperature at every nodal point.

The following dimensionless quantities are introduced

$$X = \frac{x'}{L}, \quad Y = \frac{y'}{L}, \quad Z = \frac{z'}{L}, \quad \theta = \frac{T'}{T'_{w_1}} \text{ or } \frac{T'}{T'_{w_2}}, \quad V = \frac{U'_z}{U}, \quad t = \frac{t'}{L/U}$$

$$Pr = \frac{\nu}{\alpha}, \quad Pr_t = \frac{\nu_t}{\alpha_t}, \quad Ec = \frac{\bar{U}^2}{c_p T_w}, \quad Ha = \frac{H}{2} B_m \left(\frac{\sigma_e}{\mu}\right)^{\frac{1}{2}}, \quad J = \frac{j}{\sigma_e \bar{U} B_m},$$

$$N = \frac{\bar{\kappa} k}{4\sigma T_w^3}, \quad \tau_{ox} = \bar{\kappa} H, \quad \tau_{ox} = \bar{\kappa} W, \quad Q_x = -\frac{q_x}{4\tau_{ox}\sigma T_{wx}^4},$$

$$Q_y = - \frac{q_y}{4\tau_{oy}\sigma T_{wy}^4}$$

where Pr and Pr_t = molecular and turbulent Prandtl numbers, respectively.

Ha = the Hartmann number based on the half-channel width $\frac{H}{2}$,

N = the ratio of molecular thermal conduction to radiation for a gas with an absorption coefficient $\bar{\kappa}$ and optical thickness τ_o.

Before nondimensionalizing the energy equation, it can be simplified by $U_z' >> U_x'$ and U_y' (since the velocities perpendicular to the axial direction are much smaller in low Prandtl number fluids as compared to the axial flow, even in the boundary). Therefore, the 2nd and 3rd terms on the left hand side can be neglected. Applying the nondimensional variables we have the energy equation

$$\frac{\partial\theta}{\partial t} + V\frac{\partial\theta}{\partial z} = \frac{1}{Re_t Pr_t}\frac{\partial}{\partial y}\left[(1 + \frac{Pr}{Pr_t}\frac{\nu_t}{\nu})\frac{\partial\theta}{\partial y}\right] + \frac{1}{Re_t Pr_t}\frac{\partial}{\partial x}\left[(1 + \frac{Pr}{Pr_t}\frac{\nu_t}{\nu})\frac{\partial\theta}{\partial x}\right]$$

$$+ \frac{Ec}{Re_t}(1 + \frac{\nu_t}{\nu})\left[(\frac{\partial V}{\partial y})^2 + (\frac{\partial V}{\partial x})^2\right]$$

$$+ Ha^2\frac{Ec}{Re_t}J^2 + \frac{\tau_{oy}^2}{N\cdot Re_t Pr_t}\frac{\partial Qy}{\partial y} + \frac{\tau_{ox}^2}{N\cdot Re_t Pr_t}\frac{\partial Qx}{\partial x} \quad . \tag{3}$$

For steady plasma flow between the two parallel electrode plates, y-direction variaton only, no viscous dissipation, and the plasma with a dominant conductive loss in the channel, the above equation can be written in the simple form

$$V\frac{\partial\theta}{\partial z} = \frac{1}{Re_t Pr_t}\frac{\partial}{\partial y}\left[1 + \frac{Pr}{Pr_t}\frac{\nu_t}{\nu}\frac{\partial\theta}{\partial y}\right] + Ha^2\frac{Ec}{Re_t}J^2 \tag{4}$$

The above equation, coupled with the following equations, is numerically solved by the finite difference method. The purpose of the computation was to show the temperature and the electrical conductivity profiles between two electrodes along the MHD channel, to give the power output assuming a load to be applied, and to determine the generator efficiency. The power output density, considering the effective electrical conductivity is given by:

$$P = \frac{\beta^2}{1+\beta^2}\sigma_{eff} U^2 B^2 K(1 - K) \tag{5}$$

where

$$K = (\sqrt{1 + \beta^2} - 1)\ \beta^{-2}\ .$$

The current in the MHD channel, is

$$J = \sqrt{\sigma_{eff}\ P}\quad , \tag{6}$$

and the efficiency is

$$\eta = \frac{\beta^2(1-K)}{K^{-1} + \beta^2} \tag{7}$$

Velocity

Kruger and Sonju (Ref. 2), employing the Karman-Pollhausen technique, estimated the wall shear stress and boundary-layer thickness corresponding to the semi-empirical velocity correlations proposed by Harris (Ref. 3). The local velocity normalized with the centerline value is evaluated from

$$\frac{U(\eta)}{U_c} = (\frac{C_f}{2})^{\frac{1}{2}} \left[6.154 + 2.457\ \ln\ (Re_t\ \eta) + F_1(\frac{Ha^2}{Re_t}\ \ \eta)\right] \tag{8}$$

where η is equivalent to y.

Graphical results for the asymptotic friction coefficient presented by Kruger and Sonju (Ref. 1) may be approximated by

$$\frac{C_f}{2} = \left[10.536 + 0.929\ \ln\ (\bar{B}) + 0.0222\ \ln^2\ (\bar{B})\right]\ \times\ 10^{-3} \tag{9}$$

where $\bar{B} = Ha^2/Re^2$ is the interaction parameter. The turbulent Reynolds number is defined by

$$Re_t = Re(\frac{C_f}{2})^{\frac{1}{2}} = \frac{\rho U_c L}{\mu}\ (\frac{C_f}{2})^{\frac{1}{2}} \tag{10}$$

where $0 \leq \eta \leq L$.

The function $F_1(\zeta)$ is presented graphically by Harris (Ref. 3) and may be approximated by the following expression (Ref. 2):

for $\zeta \leq 0.6$

$$F_1(\zeta) = 2.502 + 21.930\zeta - (6.359 + 53.747\zeta + 649.535\ \zeta^2)^{\frac{1}{2}} \tag{11a}$$

and

for $\zeta > 0.6$

$$F_1(\zeta) = -2.07 - 2.457 \ln(\zeta) \ . \tag{11b}$$

where the parameter ζ is equivalent to $\frac{Ha^2}{Re_t}\ \eta$.

Near the wall, when η is small, velocities evaluated from Equation (8) become negative as a result of the logarithmic term. Therefore, in a manner similar to that employed in ordinary hydrodynamic (OHD) turbulent flows for the laminar sublayer, velocities are calculated utilizing the product of $Re_t \cdot \eta$ up to the position where this product equals Equation (8). For the sublayer

$$U = L\eta\ \frac{g_c \gamma'}{\rho \nu}\ . \tag{12}$$

The sear stress on the wall is defined by

$$\gamma' = 0.0395\ \frac{\rho U_c^2}{g_c}\ \left(\frac{\nu}{4\ r_h\ U_c}\right)^{\frac{1}{4}} \quad , \tag{13}$$

where r_h is the hydraulic radius. For the rectangular cross section area of the channel, the hydraulic radius is

$$r_h = \frac{LH}{4(L+H)} \quad . \tag{14}$$

Therefore, the velocity in the sublayer is

$$\frac{U}{U_c} = 0.01757\ \left(\frac{L+H}{H}\right)\ Re_t^{\ 3/4}\ \eta. \tag{15}$$

Turbulent Viscosity

For the viscous boundary and wall heat loss, the viscosity and thermal conductivity must be considered. In most practical MHD applications, the flow is turbulent so that the transport processes are dominated by turbulent flow. Expressions for the turbulent viscosity for MHD flows are generally based on those for turbulent viscosity for the MHD flow with modifications to account for such factors as the damping of the turbulent viscosity as the magnetic field is increased.

The OHD turbulent viscosity model used by Van Driest (Ref. 4) is modified by the Mei and Squire channel factor (Ref. 5), and is utilized with a multiplicative magnetic damping function by Fiveland (Ref. 6). With these corrections,

$$\frac{\nu_t}{\nu} = \frac{0.5\ D}{1 + \bar{b}\eta} \left\{ \left[1 + 4\bar{K}^2 \bar{Z}^2 \ (1 - e^{\bar{Z}/\bar{A}})^2 \right]^{\frac{1}{2}} - 1 \right\} \quad , \tag{16}$$

and the turbulent distance, $\bar{Z}$, is defined by

$$\bar{Z} = \eta Re_t \quad . \tag{17}$$

The magnetic damping function used by Fiveland (Ref. 6) is

$$D = e^{-700\ Ha^2/Re_t^2} \tag{18}$$

Thermal Conductivity

In a plasma, unlike the case of viscosity, the internal structure of the colliding particles play an important role in determining the thermal conductibity. This is due to the fact that energy may be stored in internal degrees of freedom such as rotation, vibration, and electronic excitation. In a mixture, which is in thermal equilibrium, particles recombine when they move against a temperature gradient and then release the energies of dissociation or ionization. However, the kinetic theory provides the simplest methods for estimating the transfer coefficients for a single component, monoatomic gas. Denoting the particle concentration by n_e, the mass of the particles by m_e, and the effective collision cross section for a solid sphere molecular model $\overline{Q(T)}$, the coefficient of thermal conductivity for ionized gas is described by

$$k = \frac{25}{16} \frac{\sqrt{\pi m_e \kappa T}}{\overline{Q(T)}} \cdot \left(\frac{\kappa}{m_e}\right) \tag{19}$$

The equation describes the thermal conductivity which would be valid if the composition of dissociated gas were frozen. That is, the processes are ideally faster than any chemical kinetic process.

In Equation 19, the collision cross sections, $\overline{Q(T)}$, for rigid spherical molecules of diameter D is equal to $\frac{2}{3}\pi D^2$. This relationship can be used to estimate $\overline{Q(T)}$ for collisions between like molecules.

Electrical Conductivity

The current density in the MHD channel is proportional to the electrical conductivity of the working medium. The formulation of current density, j, in the channel is given

$$j = \sigma U_z B(1 - K) \tag{20}$$

where K is the generator coefficient and σ is the electrical conductivity. The electrical conductivity is related to the electron density, n_e, and the mobility, μ, of the gas by a general form (Ref. 7):

$$\sigma = n_e e\mu \quad . \tag{21}$$

For MHD generators using alkali seeded noble gases as working fluids, non-equilibrium ionization occurs when Joule heating of the gas by the current causes the electron temperature, T_e, to be higher than the gas temperature, T_g. To compute the electrical conductivity, taking into account the non-equilibrium ionization in MHD generators, the effective electrical conductivity rather than the scalar conductivity has to be used in the basic MHD equations.

The effective conductivity is given by Zampaglione (Ref. 8) as

$$\sigma_{eff} = \frac{\sigma[(\beta - \bar{\xi})^2 + (\beta\bar{\xi})^2]}{\beta[\beta + \bar{\xi}(\beta^2 - 1)]} \tag{22}$$

where β is the Hall parameter and $\bar{\xi}$ is a plasma turbulence factor ranging from 0.5 to 1.0. The Hall parameter is

$$\beta = \mu B \quad . \tag{23}$$

The electron mobility, μ, is given by

$$\mu = \frac{e}{m_e \nu_2} \tag{24}$$

where ν_2 is the collision frequency of electrons and neutrals.

To calculate the electron density, n_e, Saha's equation is modified because $T_e > T_g$ and the effective ionization potential of the seed is lowered by the Debye cloud. The modified Saha's equation for n_e (Refs. 9, 10 and 11) is

$$n_e = (K_1 \bar{C})^{\frac{1}{2}} \left[\left(\frac{K_1\bar{\beta}^2}{4\bar{C}} + 1\right)^{\frac{1}{2}} - \left(\frac{K_1\bar{\beta}^2}{4\bar{C}}\right)^{\frac{1}{2}} \right] \tag{25}$$

where

$$\bar{\beta} = \left(1 + \frac{T_e F}{T_g(1+F)}\right) ,$$

$$\bar{C} = \frac{Fp}{(1+F)\kappa T_g} ,$$

$$K_1 = \frac{2\, Z_s^+}{Z_s^o} \frac{(2\pi m_e \kappa T_e)^{3/2}}{h'^3} \exp\left[-e\,(V_o - \gamma)/\kappa T_e\right] .$$

In these equations, F is the mole fraction of the seed, p is the total pressure, Z_s^+ is the electronic partition function of the seed ion, Z_s^o is the partition function of the seed neutrals, h' is Plank's constant, V_o is the ionization potential, and γ is the lowering of the ionization potential by the Debye cloud. The lowering factor of the ionization potential by the Debye cloud is defined by

$$\gamma = \frac{Z\, e^2}{4\pi\, \varepsilon_o\, \rho_d} . \tag{26}$$

The Debye radius is given by

$$\rho_d = \sqrt{\frac{\varepsilon_o \kappa T_e}{2\, e^2\, n_e}} \tag{27}$$

where z = 1 for atoms, 2 for + ions, and 3 for ++ ions, and ε_o is the permitivity of free space.

The degree of ionization is given by

$$a = \frac{n_e}{(n_B + n_{Cs})} \tag{28}$$

where n_B is the density of He or Ar. The collision frequency for He, as a function of a, is then defined by the approximation (Ref. 12),

$$\nu_2 = \left[3.10 + (8085\ a - 0.2264)^{0.71}\right] \times 10^{-14}\ n_{He} , \tag{29}$$

if (8085 a - 0.2264) > 0. Equation (29) becomes

$$\nu_2 = 3.10 \times 10^{-14}\, n_{He}, \text{ if } (8085\, a - 0.2264) < 0. \tag{30}$$

For Ar

$$\nu_2 = \left[0.53 + 0.641 \times (10^4\, a)^{0.72}\right] \times 10^{-14}\, n_{Ar} \quad , \tag{31}$$

where n_{He} and n_{Ar} are here in units of particle/cm^3.

The initial electron temperature at the entrance of the MHD channel can be defined by solving a set of equations describing the laser-plasma interaction. The electron temperature in the MHD channel can be replaced by the plasma gas temperature which is implicitly computed by a set of equations for the MHD channel. In this simplified model, the entrance electron temperature was set at 2500 K.

RESULTS

The breakdown threshold for plasma production by laser radiation depends on the medium pressure (Fig. 3), the focal volume (Fig. 4), the peak irradiance (Figs. 5 and 6), and the absorption band (Fig. 7). The growth of plasma beyond the breakdown threshold, however, depends entirely on absorption which falls into two different catagories, namely, short and long pulses (Ref. 1). In a single short pulse region, inverse bremsstrahlung comprises about 40% absorption. On the other hand, in a long pulse, absorption of over 80% occurs up to the point where the transition from classical to anomalous behavior begins. Beyond the transition point, the absorption rapidly drops to about 50% due to the ion-acoustic turbulence, the Brillouin backscatter, the specular reflection, and the non-linear behavior of the plasma. The absorption of high laser irradiance in the long pulse mode by an expanding plasma ball can be improved by a well-designed interaction chamber. The specular reflection and the scattering at the critical density surface of the plasma comprise about 40% of the total irradiance in the long pulse mode. Such losses are sensitive to the laser power level and can be partly retrieved by considering the design of the optics and geometrical configuration, magnetically controlled plasma boundary, and by fabricating the plasma chamber with highly reflective surfaces. That is, well-designed optics and a geometry configuration with highly reflective surfaces can refocus the beam reflected from the plasma surface back to the plasma. The damage to the reflective chamber walls can also be alleviated by magnetically controlling the plasma boundary. In this case, the total absorption would be above 80% at the peak irradiance of a long pulsed laser. This is the optimized value of the conversion efficiency of the laser incident beam energy as shown in Figure 2.

The characteristics of this absorption mechanism, as well as the crucial effect of the cold boundary, have to be accounted for in the plasma expansion, since the possibility exists that the plasma would decay before passing through the MHD generator. Applying a magnetic field to pinch the plasma radially until the plasma passes through the generator may solve the cold boundary problem, or, on the other hand, alleviates the damage to the wall by the highly expanding plasma. The magnetic field may be used to thermally insulate the plasma from the cold wall. Since the cold wall is in contact with the plasma, it induces intabilities which enhance thermal conduction losses (Ref. 13). Table VI describes the laser sources, the medium, the breakdown threshold, the plasma temperature, the focal volume, and more. More research is needed to establish the dynamics and characteristics of the laser-induced plasma with respect to the irradiant power, the time to breakdown, growth, decay, the total absorption, and the medium pressure. How effectively the laser energy can be used to produce a plasma in a chamber of improved geometrical features with specific radiative properties should also be investigated.

The power density and the system efficiency of the MHD cycle is much higher compared to those of the conventional thermal cycles. However, the main problems in the development of MHD generators are the high temperatures required and the corrosive gas medium which can easily damage the electrodes and wall of the generator.

Though well-known concepts and well-developed analysis exist, the MHD generators still require intensive research for use in space. The existing analysis related to the conventional MHD generator may not be sufficient for the direct application to the laser-driven plasma MHD system because the energy source is in the form of a light beam. The light beam not only penetrates the plasma production chamber, but also extends the energy input through the generator, and thus may deposit the input energy unevenly throughout the plasma.

From a simplified model computation, the temperature, velocity, and electrical conductivity distribution were obtained. These distribution curves from the center of the channel to the electrode at different points along the axial direction are shown in the Figures 9, 10, 11, and 12. The variables were non-dimensionalized so that the numbers in the figures are described with the scaled values. The velocity profile in Figure 9 was obtained with the assumption of a turbulent channel flow. This approach is reasonable, since the MHD flow usually has a turbulent flow profile. Based upon the velocity profile, the temperature and electrical conductivity for the medium were calculated. The temperature profiles in Figure 10 are scaled by the uniform wall temperature. By considering the electron mobility and plasma turbulences with the above velocity and temperature profiles, the effective electrical conductivity was computed and is shown in Figure 12. The electrical conductivity is significantly affected (as much as 55 percent) by the electron mobility and the plasma turbulence (which is also a function of temperature). From the above computational results, the average values of velocity, temperature, and effective electrical conductivity are obtained. These average values can be used to calculate the Hall parameter and the generator coefficient which are, in turn, used to calculate the power output density and the efficiency. The power output density and the efficiency considering the electron mobility and plasma turbulence was 0.2254 W/cm^3 and 43 percent. These values can be improved by optimizing the design of the channel. For the same power output density, an efficiency of 54 percent is calculated based on the electron density of 1.315 x 10^{19}/cm^3, the medium average temperature, 2500 K, and ignoring turbulent effects and non-equilibrium ionization. Table VII shows the parameters of a MHD generator used for the two cases.

CONCLUSIONS

In conclusion, the literature survey and the simplified model calculations show that based on its efficiency and power density, the laser-driven MHD system is practical and may have applications for future spacecraft energy system in space.

From the simplified model the generator efficiency is 53.5 percent, if turbulence and non-equilibrium ionization are ignored. If these effects are taken into account, the efficiency is reduced to 43.2 percent.

Further detailed theoretical and experimental analysis of the laser-driven MHD generator are necessary to realize a high potential for space application.

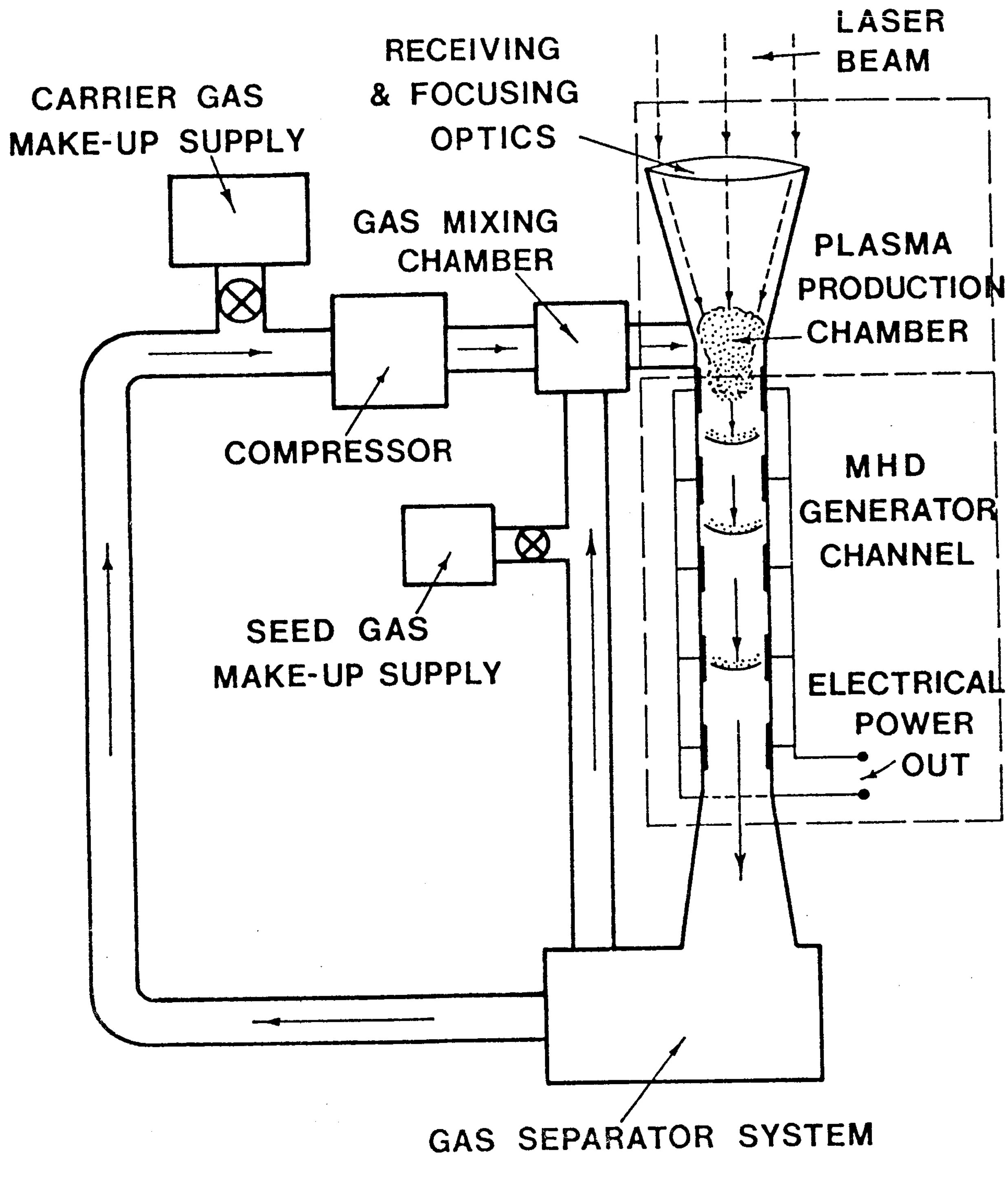

FIGURE 1. LASER-DRIVEN MHD GENERATOR

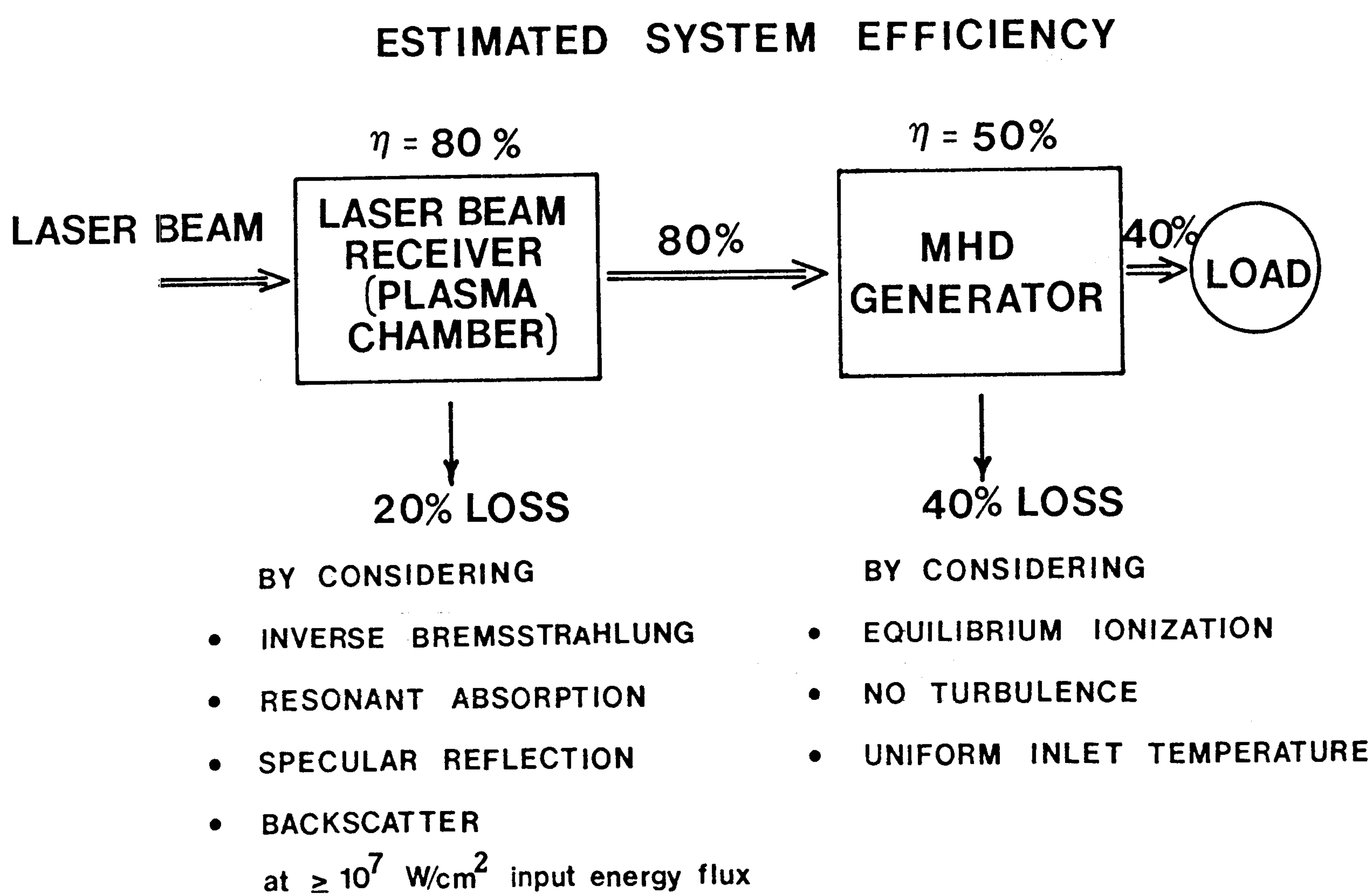

FIGURE 2. LASER-DRIVEN MHD SYSTEM EFFICIENCY BLOCK DIAGRAM

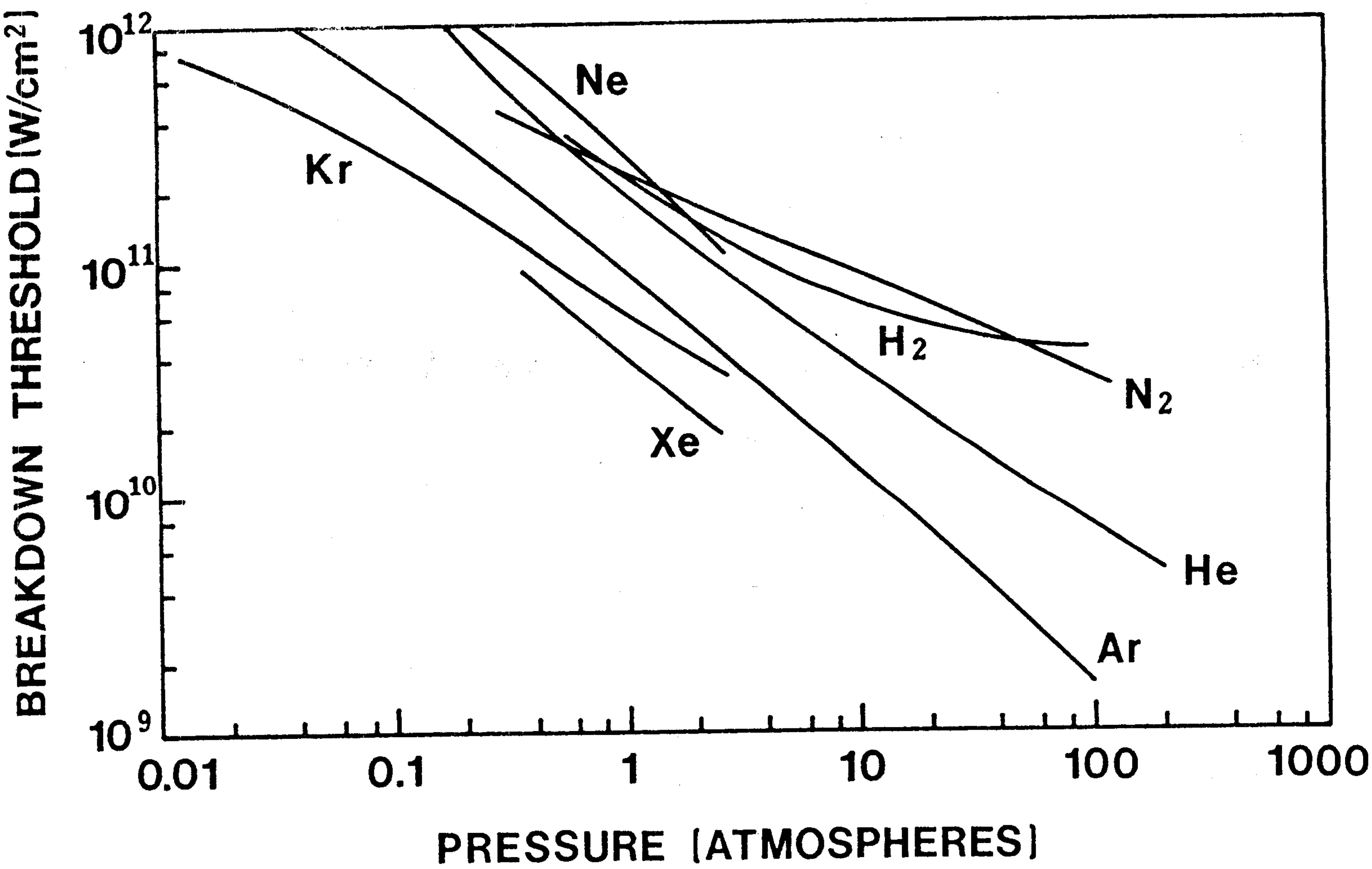

FIGURE 3. A COMPILATION OF THE EXPERIMENTAL RESULTS ON BREAKDOWN THRESHOLD AS A FUNCTION OF PRESSURE FOR A NUMBER OF GASES. (REF. 52)

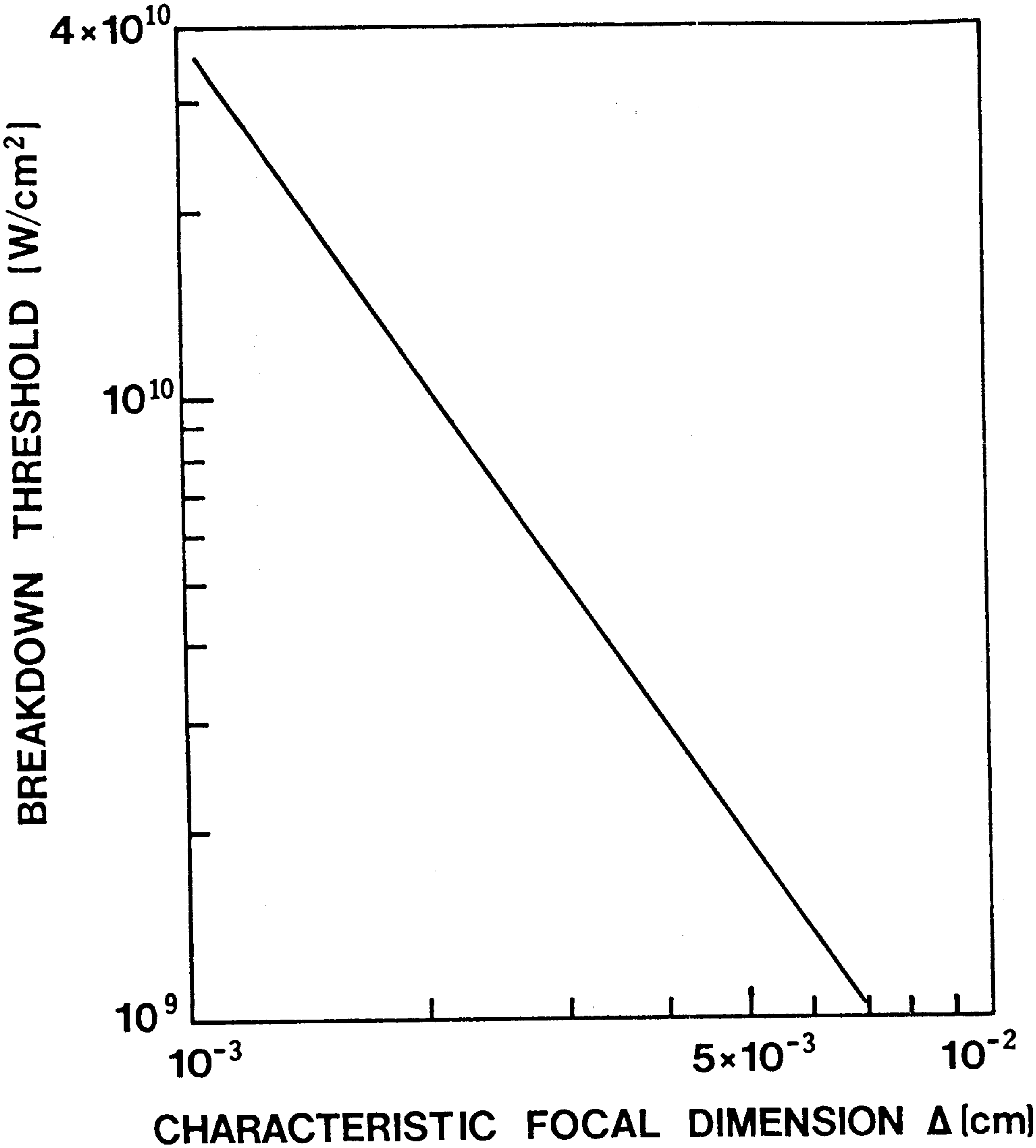

FIGURE 4. BREAKDOWN THRESHOLD FOR Ar (PRESSURE 5.2 x 10^4 TORR) AS A FUNCTION OF CHARACTERISTIC FOCAL DIMENSION Δ. (REF. 53)

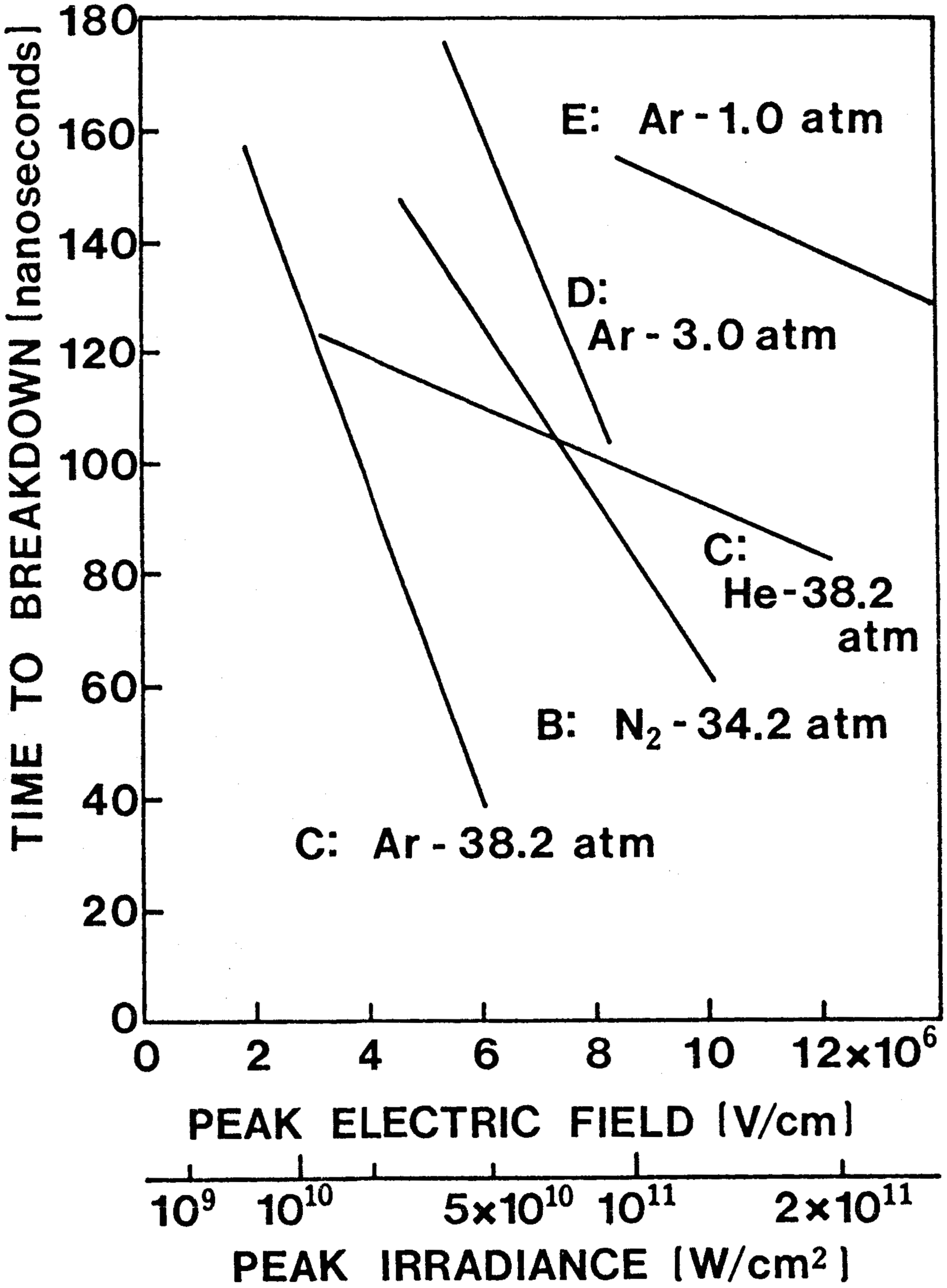

FIGURE 5. BREAKDOWN TIME AS A FUNCTION OF PEAK IRRADIANCE AND PEAK ELECTRIC FIELD FOR A Q-SWITCHED RUBY LASER PULSE FOCUSED IN VARIOUS GASES. (REF. 54)

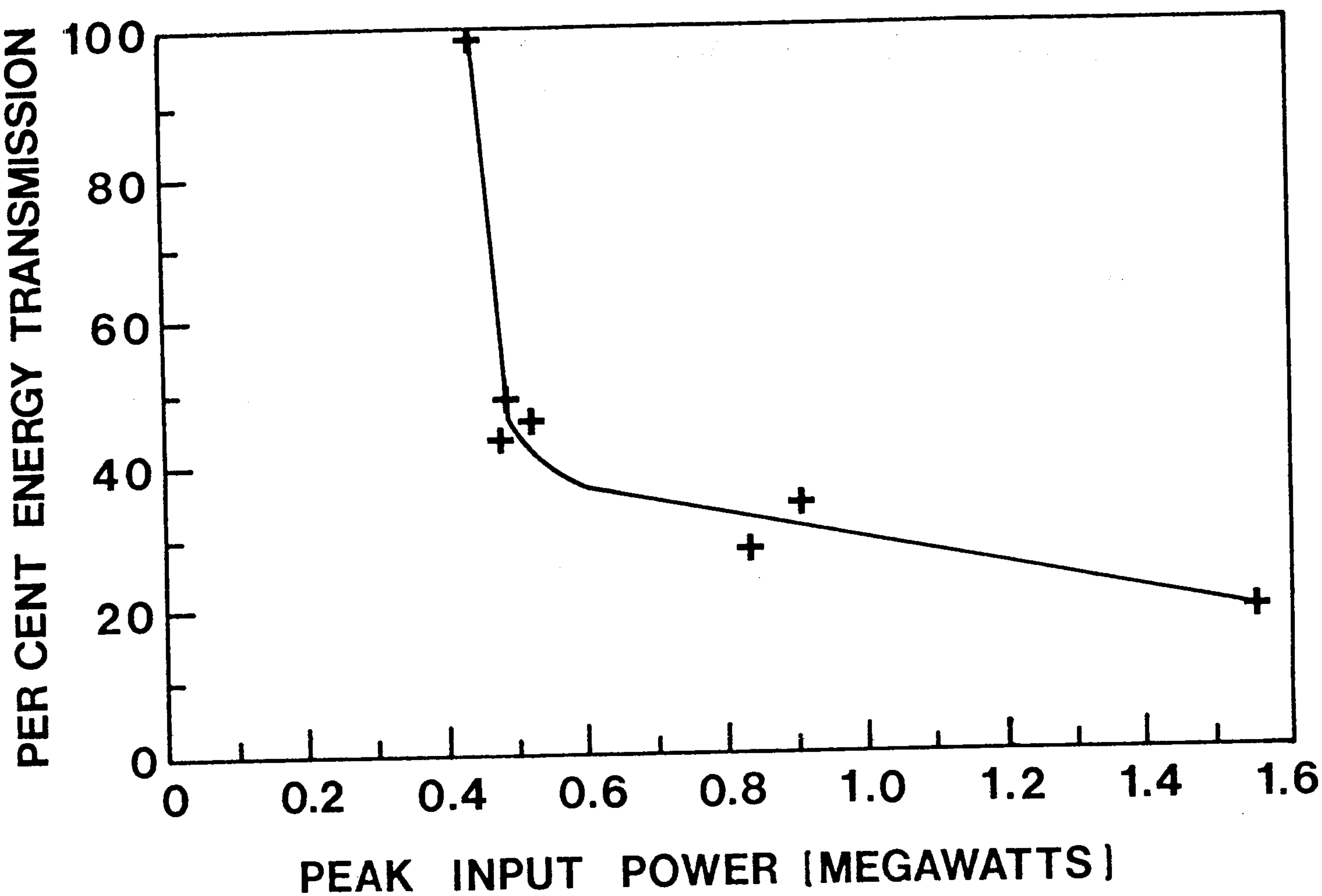

FIGURE 6. OPTICAL TRANSMISSIVITY OF AIR AT A PRESSURE OF 746 TORR AS A FUNCTION OF PEAK POWER IN A RUBY LASER PULSE FOCUSED BY A 2.06 - cm FOCAL LENGTH LENS. (REF. 55)

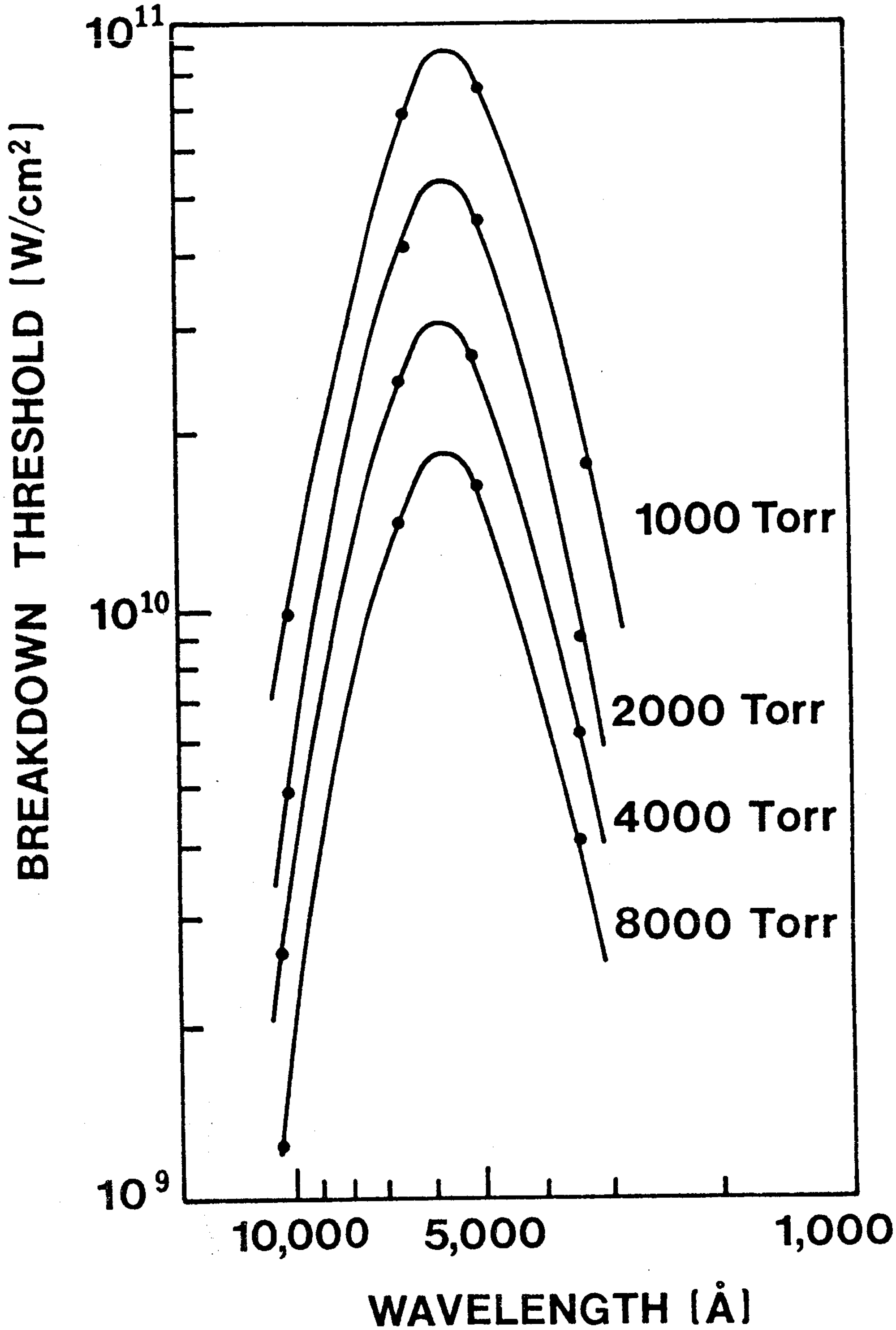

FIGURE 7. BREAKDOWN THRESHOLD AS A FUNCTION OF WAVELENGTH OF INPUT RADIATION FOR Ar AT FOUR SELECTED PRESSURES. (REF. 56)

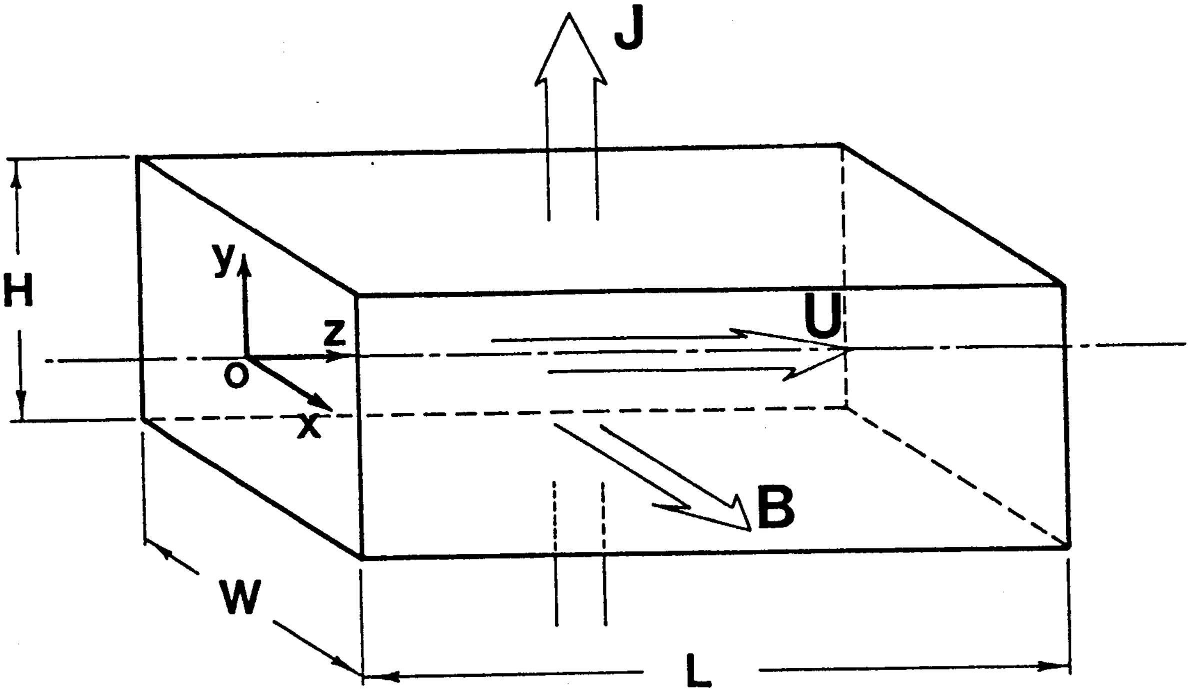

FIGURE 8. MHD CHANNEL

J is the current density along the y direction

B is the magnetic flux along the x direction

U is the velocity along the z direction

H is the height of the generator between electrodes

W is the width of the generator

L is the length of the generator

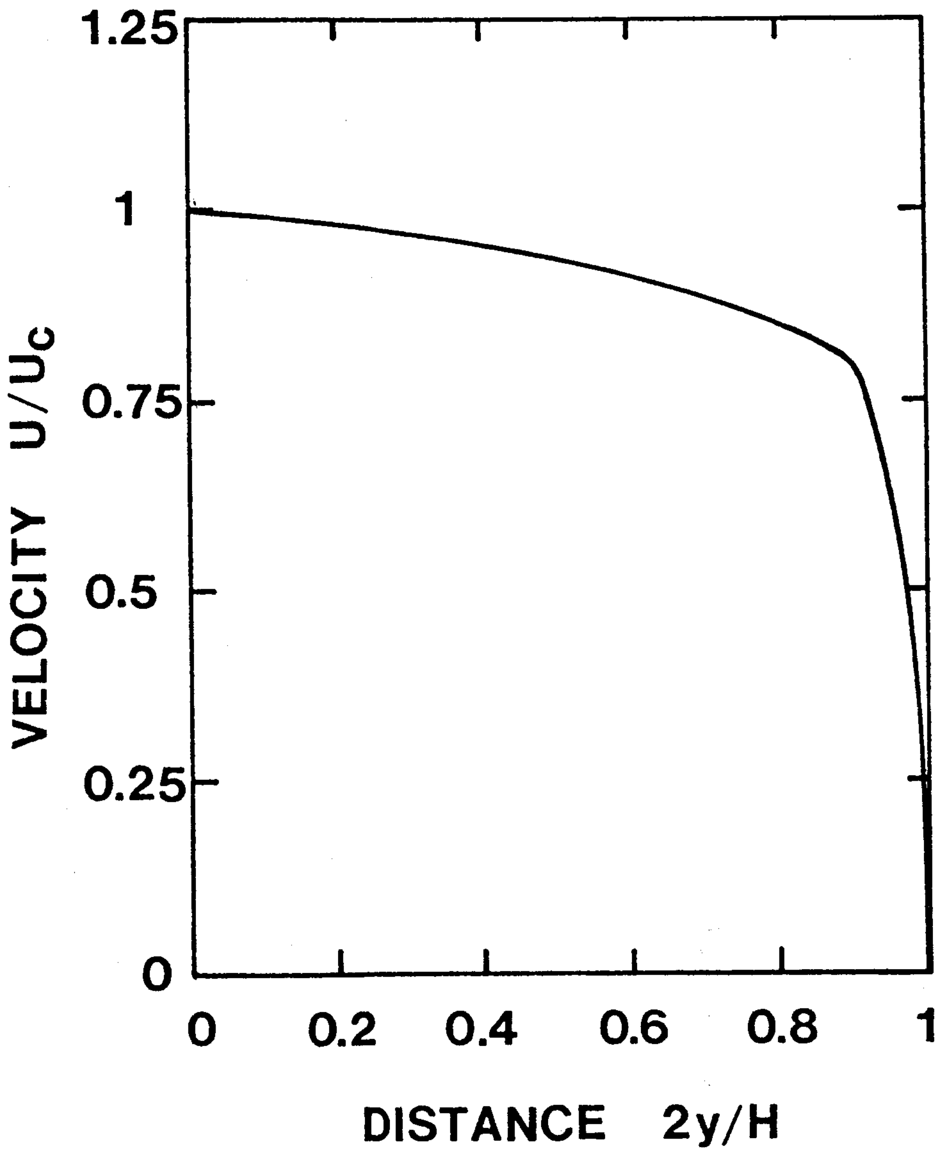

FIGURE 9. CALCULATED VELOCITY PROFILE OF TURBULENT FLOW IN THE MHD CHANNEL

The velocity is the ratio of a local velocity based on the velocity U_c at the axial center of the generator

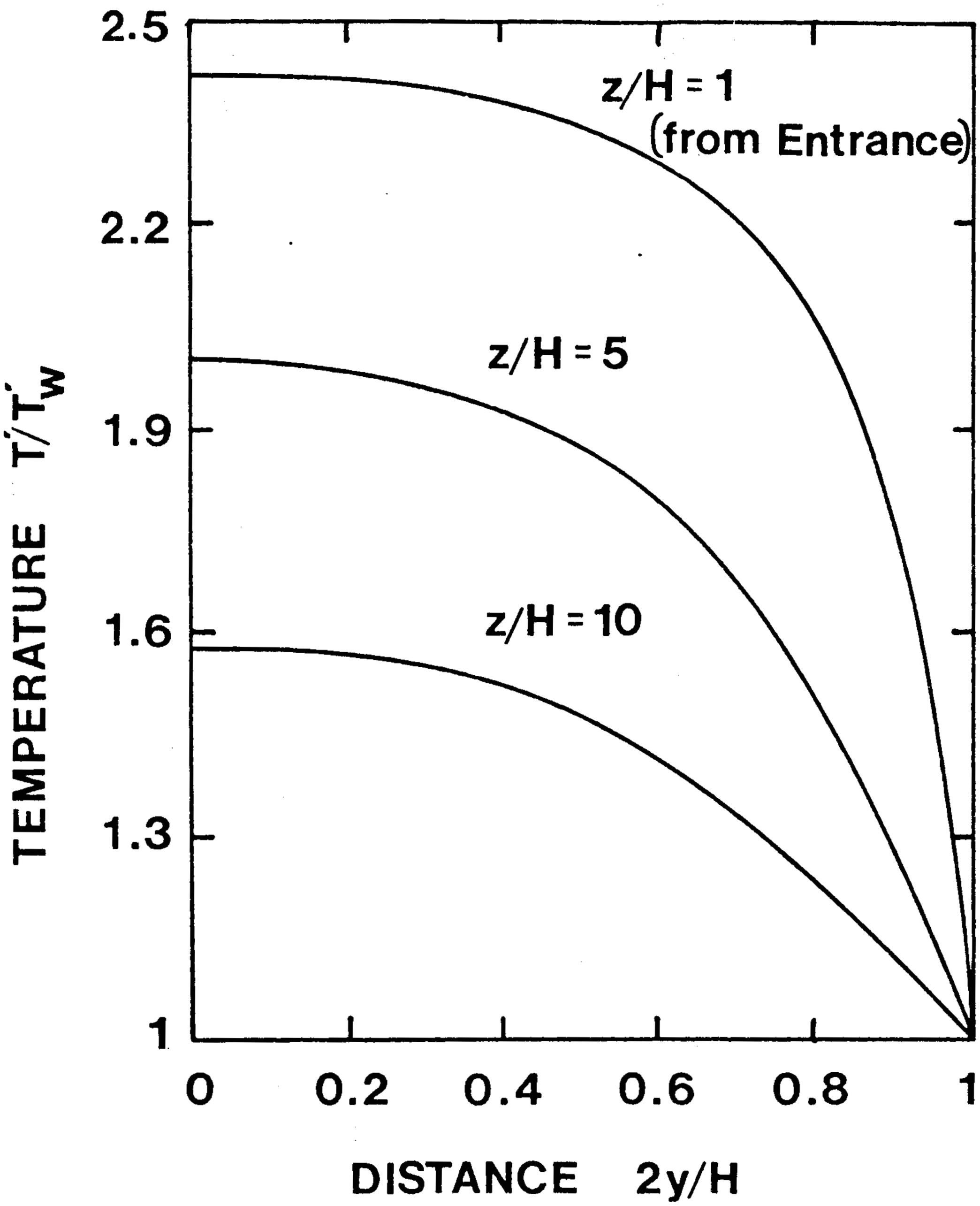

FIGURE 10. CALCULATED TEMPERATURE PROFILES AT THREE DIFFERENT LOCATIONS FROM THE ENTRANCE OF THE MHD CHANNEL

The constant wall temperature of 1000 k was used in the calculation

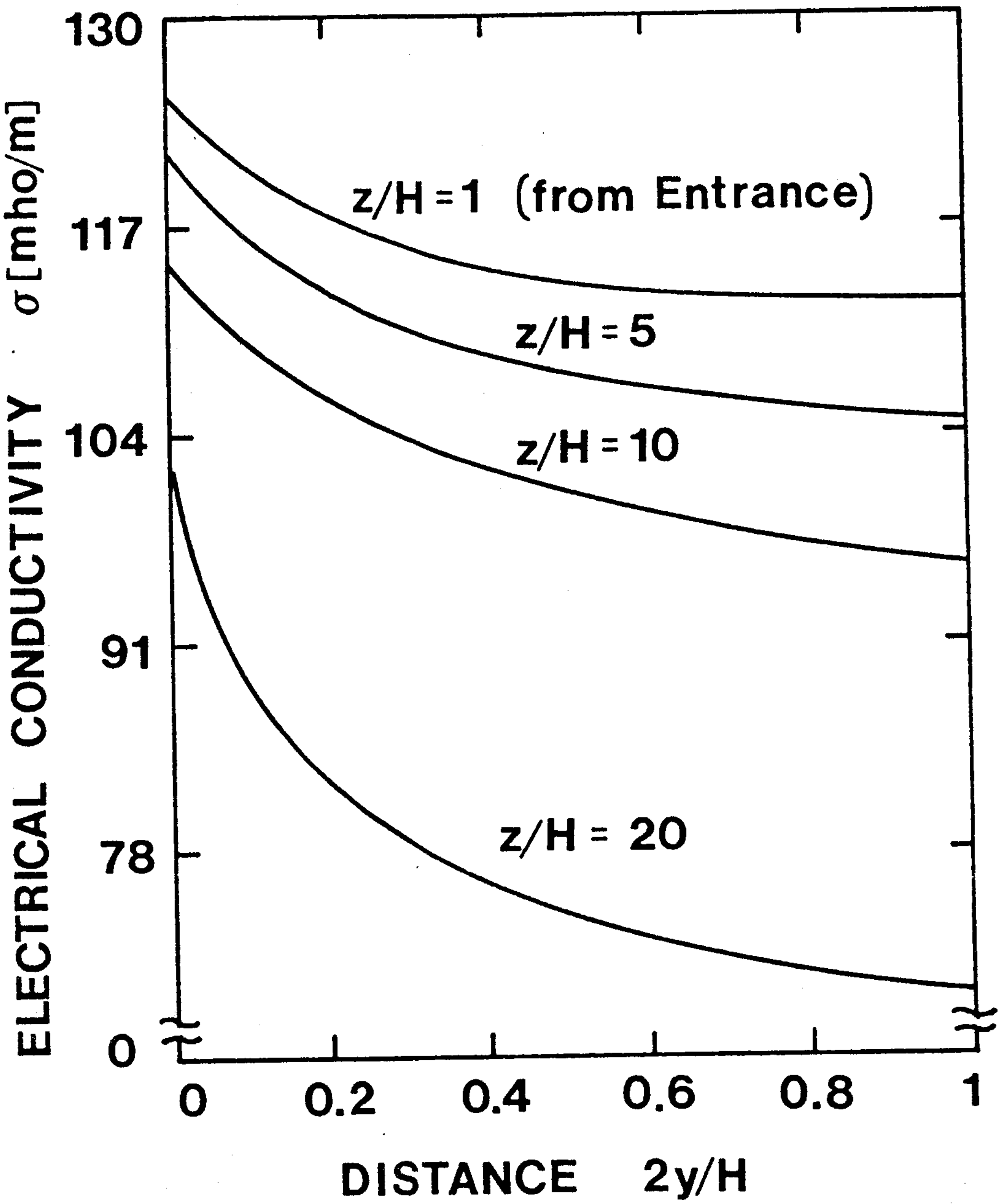

FIGURE 11. CALCULATED ELECTRICAL CONDUCTIVITY PROFILES AT FOUR DIFFERENT LOCATIONS FROM THE ENTRANCE OF THE MHD CHANNEL

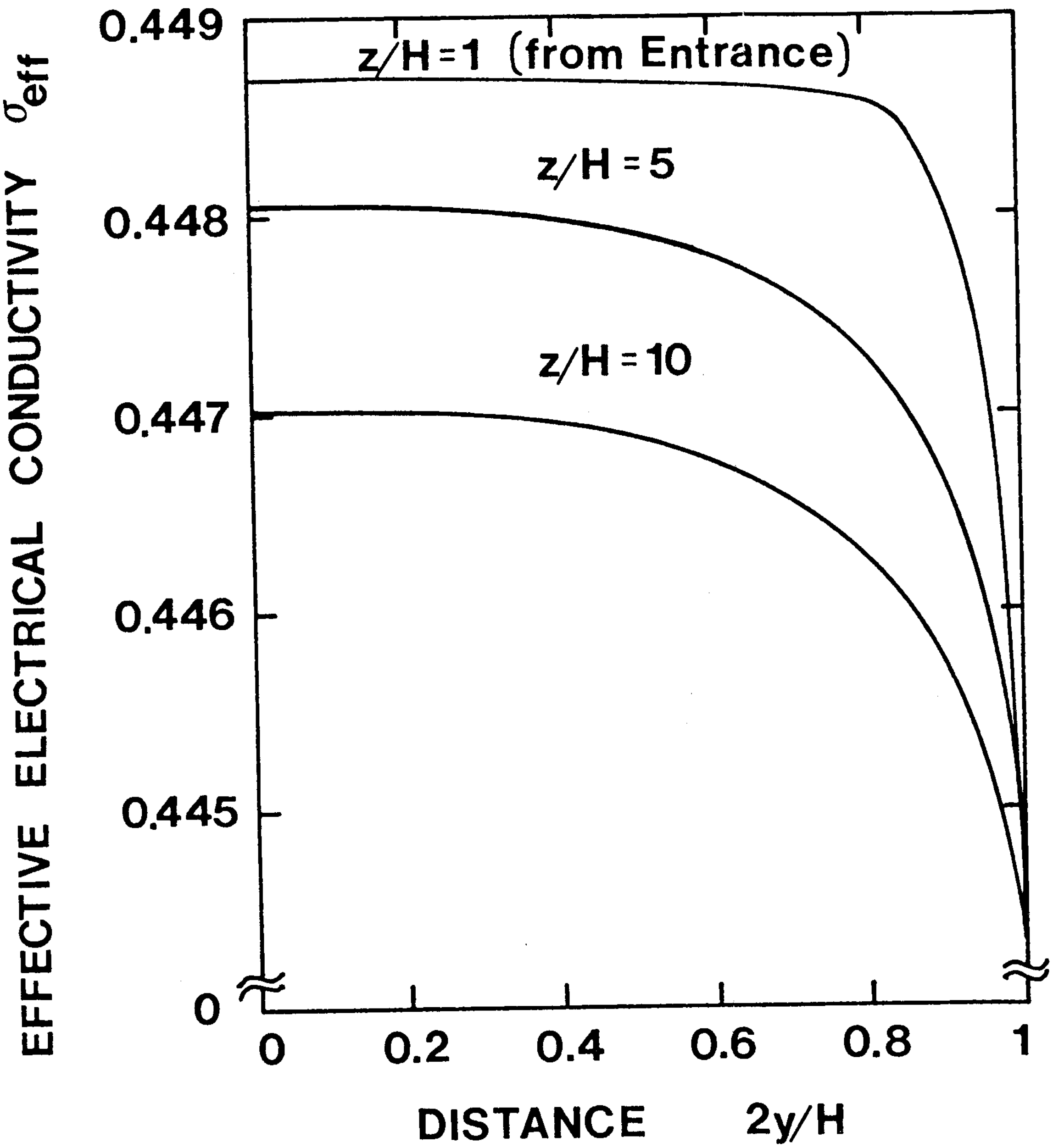

FIGURE 12. CALCULATED EFFECTIVE ELECTRICAL CONDUCTIVITY PROFILES AT THREE DIFFERENT LOCATIONS FROM THE ENTRANCE OF THE MHD CHANNEL

TABLE I. PLASMA MHD

MODEL	CHARACTERISTICS OF SYSTEMS	MHD CHANNEL WORKING FLUID FLUID	GENERATOR TYPE	FLOW RATE kg/s	VELOCITY m/s	TEMPERATURE IN/OUT K	CONDUCTIVITY mho/m	POWER OR POWER DENSITY	DIMENSION H x W x L
UT HYBRID ROCKET PLASMA MHD	COMPACT HIGH POWER	PLASMA (SEEDED SOLID FUEL)	FARADAY OR HALL	2.27	1700	4500/3500	170	1600 W/cm^3	
AVCO, SHOCK DRIVEN DISK HALL	LARGE DRIVEN IN A SHOCK TUBE	HIGH TEMPERATURE PLASMA	DISK HALL	11	1000	4000/1600	NA	720 kW	NA
GE, SHOCK DRIVEN LINEAR MHD	LARGE, NON-EQU. SHOCK DRIVEN	SHOCK HEATED Xe - PLASMA	LINEAR SEGMENTED FARADAY	NA	985	4960	75	600 700 kW	0.05 m x 0.05 m x 1.52 m
BMI, NUCLEAR & SHOCK DRIVEN MHD	LARGE SHOCK DRIVEN	NUCLEAR HEATED He - PLASMA	NA	348	1415	3280	200	683 W/cm^3	18.5 cm x 10^4 cm x 573 cm
AVCO, COMBUSTION DRIVEN LINEAR HALL	COMBUSTION	COMBUSTION PLASMA	HALL	2 - 3.6	2250	2450	4.5	2 MW	(5 cm x 16.6 cm) in x (15 cm x 24.9 cm) out x 175 cm
UTSI, LINEAR HALL	45° DIAGONAL CONDUCTING	COMBUSTION PLASMA	HALL	NA	1600	1300	23	NA	(2" x 4" 2" x 6") x 36 "
SU EXPERIMENT III	SMALL COMBUSTION	COMBUSTION PLASMA	SEGMENTED FARADAY	3	2000	2700	14	1 MW	(83 cm^2) in (335 cm^2) out L - 150 cm
NASA-LEWIS	ARC.	Ar - PLASMA	FARADAY	1.8	350	2050	8	NA	19 cm x 6.35 cm x 195 cm
ODU EXPLOSIVE DRIVEN MHD	EXPLOSIVE DRIVEN PULSED MHD	PLASMA BY EXPLOSION	FARADAY	1070 m^3/s	18500	30000	10^4	(0.03 MW) 428 MW * (21 MW)	2.6 cm x 1 cm x 0.75 cm
ARGAS I SWISS	CLOSED LOOP	PLASMA	HALL	2.7	600	1735/1440	2.6	2 W/cm^3	NA
MIT	NON-EQU. 45° SLANTED ELECTRODE WALL	BLOW DOWN PLASMA	FARADAY	0.4	NA	2000/800	NA	NA	NA
DETONATION MHD USSR	COMPACT HIGH POWER	DETONATION WAVE DRIVEN PLASMA	SEGMENTED FARADAY	300 m^3/s	2380	3700/3575	75	0.01 W/cm^2 13.4 W/cm^3	16 cm x 16 cm
GE, COAL FIRED MHD	WITH FLUIDIZED BED	COMBUSTION PLASMA	FARADAY	51.73	NA	2760	11.93	250 MWt	NA
U-25B USSR	LARGE COAL BURNING	COMBUSTION PLASMA	FARADAY	5	SUBSONIC	2700 - 2900/	NA	MHD alone 10 W/cm^3	2.4 cm x 7.6 cm x 506.4 cm
INDIAN MHD X	SMALL GAS BURNING	COMBUSTION PLASMA	FARADAY	1	800	2840	15.3	5 MW	NA
EINDHOVEN MHD	BLOW DOWN DRIVEN	SHOCK DRIVEN PLASMA	FARADAY	5	M = 1.6	2000	NA	5 MW	(5 cm x 15 cm) in (18 cm x 15 cm) out x 80 cm

TABLE I. PLASMA MHD (CONCLUDED)

MODEL	NUMBER OF ELECTRODE OR CONDUCTOR	EFFICIENCY	MAGNETIC FIELD STRENGTH TESLA	CYCLE	SEED MATERIAL	WORKING FLUID FUEL/OXIDIZER	RUNNING MODE	ELECTRON DENSITY	SOURCE REFERENCE
UT HYBRID ROCKET PLASMA MHD	NA	NA	4	OPEN	CESIUM NITRATE	RUBBER BASED RUEL/D_2	30 SEC PULSE	NA	REF. 14
AVCO, SHOCK DRIVEN DISK HALL	1 PAIR	NA	3.2	OPEN	CESIUM	NA	2 mS	NA	REF. 15
GE, SHOCK DRIVEN LINEAR MHD	30	0.16 (?)	2.2/7.35	OPEN	NONE	9.2% CO 90.8% Xe	NA	3.75×10^{14}	REF. 16
BMI, NUCLEAR & SHOCK DRIVEN MHD	NA	0.52 (?)	5	OPEN	CESIUM	HELIUM	NA	NA	REF. 17
AVCO, COMBUSTION DRIVEN LINEAR HALL	NA	0.14	2.3 - 3.3	OPEN	Cs_2CO_3 OR K_2CO_3	TOLUENE/OXIDIZER	5 - 8 SEC PULSE	NA	REF. 18
UTSI, LINEAR HALL	60	NA	2.1	OPEN	KOH	RPI/OXIDIZER	CONTINUOUS	10^{16}	REF. 19
SU EXPERIMENT III	3	NA	3	OPEN	KOH	NA	15 SEC PULSE	NA	REF. 20
NASA-LEWIS	28	0.66	1.8	CLOSED	CESIUM (1.5 - 3 g/sec)	ARGON	CONTINUOUS	NA	REF. 21
ODU EXPLOSIVE DRIVEN MHD	NA	>0.05	2.0	OPEN	NA	RDX*	7 μSEC PULSE	10^{24}	REF. 22
ARGAS I SWISS	20	0.17	1.3	CLOSED	CESIUM	ARGON	CONTINUOUS	NA	REF. 23
MIT	23	NA	1.25	NA	CESIUM	HELIUM	15 SEC PULSE	NA	REF. 24
DETONATION MHD USSR	NA	0.079	5	OPEN	NA	$CH_4 + O_2$	50 μSEC PULSE	NA	REF. 25
GE, COAL FIRED MHD	NA	NA	4 - 6	OPEN	K_2CO_3	NATURAL GAS/O_2	CONTINUOUS	NA	REF. 26
U-25B USSR	NA	NA	4 - 5	OPEN	K_2CO_3	NATURAL GAS/O_2	CONTINUOUS	NA	REF. 27
INDIAN MHD X	NA	NA	2	OPEN	K_2CO_3	COAL GASIFICATION/O_2	CONTINUOUS	NA	REF. 28
EINDHOVEN MHD	NA	0.21	5	CLOSED	CESIUM (0.1%)	ARGON	11 SEC PULSE	$10^{14}/cm^3$	REF. 29

TABLE II. LM MHD GENERATOR

NAME OF LM MHD	MHD WORKING FLUID	MHD GENERATOR TYPE	FLOW RATE kg/s	VELOCITY IN/OUT OR AVERAGE m/s	TEMPERATURE IN/OUT OR AVERAGE K	CONDUCTIVITY mho/m	CURRENT DENSITY	POWER OUTPUT	DIMENSION, METER H x W x L OR D x L
JPL, I SINGLE WAVE INDUCTION	LM MHD Cc + Li	AC INDUCTION	48 - 90	60 - 160 L/G = 5 - 50	1373 °K	3.185×10^6	30 AMP	500 kW	0.0159 m dia x 0.15 m
AI 1966 EXPERIMENT	LM MHD NaK	AC INDUCTION	8.62	37.88	ROOM TEMP.	2.5×10^6	45	2 - 4 kW	0.003175m x 0.0635 m x 0.602 m
ANL, TWO-PHASE D. C. LM MHD	He/Na VOID = 0.65/0.805	NA	7.5×10^4 $cm^3/sec(N_a)$	15.24	1500	2.6×10^6	3646 AMP	5.750 kW	0.0141 m x 0.10 m x 0.385 m
JPL, II	LM MHD $NaK-N_2$	NA	NaK 46 - 72 N_2 2.4 - 3.8	96/76	NA	2×10^7	15480 AMP	31 kW	0.063 m x 0.0166 m x 0.205
JPL, III BINARY	Cs + Li	BINARY CYCLE	NA	NA	1250/840	NA	NA	2500 MWt	NA
JPL IV INDUCTION	LITHIUM	INDUCTION	83	128/71	373	2×10^6	NA	325 kW	(0.66 - 1.19) cm x 22 cm x 28 cm
ANL HT-1	LM MHD Na/N_2	HIGH TEMP.	Na: 25.96 N_2: 0.177	15.24	480 - 810	2.5×10^6	NA	NA	10.16 cm x (5.09-6.86) cm x 56.52 cm
ANL LT SOLAR	LM MHD NaK-FREON 113 VOID: 0.8	LOW TEMP. INDUCTION	NA	30	298 - 353	NA	NA	50 kW	7.5 cm x 3.5 cm x 30 cm

ESTIMATED DATA FOR LASER-DRIVEN MHD GENERATORS

LaRC LASER-DRIVEN PLASMA-MHD	LASER PRODUCED PLASMA Cs + Ar(or He)	HALL	0.02 - 0.5	100 - 2500	2000 - 2500	~ 20	20 - 50 kA/m	2.35×10^2 W/cm^3 5.86 kW	(0.01 m x 0.01 m) x 0.15 m or (0.025 m x 0.025m) x .15 m
LaRC LASER-DRIVEN LM-MHD	Cs + Li	INDUCTION	~ 10	~ 25	500	3.1×10^6	3 kA/m	~ 3 kW	0.02 m x 0.010 m x 0.20 m

TABLE II. LM MHD GENERATOR (CONCLUDED)

NAME OF LM MHD	NUMBER OF ELECTRODE OR CONDUCTOR	FREQUENCY H_z	NET GENERATOR EFFICIENCY	GROSS ELECTRICAL EFFICIENCY	MAGNETIC FIELD STRENGTH TESLA	CYCLE	SEED	RUNNING TIME	SOURCE REFERENCE
JPL, I SINGLE WAVE INDUCTION	8	710	0.09	0.45	NA	CLOSED	NA	NA	REF. 30
AT 1966 EXPERIMENT	NA	200 - 400	NA	0.428	0.35	CLOSED	NA	30 SEC	REF. 31
ANL, TWO-PHASE D. C. LM MHD	NA	NA	0.18	NA	1.2	CLOSED ERICSSON	Na	NA	REF. 32, 33
JPL, II	12	270 - 470	NA	0.41	NA	NA	NA	NA	REF. 34
JPL, III BINARY	NA	NA	0.15	NA	NA	NA	NA	NA	REF. 35
JPL IV INDUCTION	NA	388	NA	0.626	2	CLOSED	Li	CONTINUOUS	REF. 36
ANL HT-1	NA	NA	NA	0.65	0.75	CLOSED	Na	CONTINUOUS	REF. 37
ANL LT SOLAR	NA	NA	0.043	0.70	0.2	CLOSED RANKINE	NaK	CONTINUOUS	REF. 38

ESTIMATED DATA FOR LASER-DRIVEN MHD GENERATORS (CONCLUDED)

LaRC LASER-DRIVEN PLASMA-MHD	8 - 20	NA	0.1	0.40	1 - 2	SIMPLE CLOSED	Cs	CONTINUOUS	PRELIMINARY DESIGN ESTIMATION BY THIS STUDY
LaRC LASER-DRIVEN LM-MHD	NA	~ 400	0.1	0.5	1 - 2	CLOSED	Cs+K	CONTINUOUS	PRELIMINARY DESIGN ESTIMATION (PROJECTED)

TABLE III. ALKALI METAL PARAMETERS

GAS	RESONANCE RADIATION WAVELENGTHS (A)	IONIZATION POTENTIAL (eV)	PERCENT IONIZATION T=2500 K, P=760 torr	LENGTH FOR 90% ABSORPTION T=2500 K, P=760 torr
POTASSIUM	7665 7669	4.45	3.3	52 cm
CESIUM	8521 8944	3.87	12.	50 cm
SODIUM	5890 5896	5.12	0.7	50 cm

TABLE IV. LASER-PLASMA INTERACTION

LASER SOURCE	MATTER GAS/SOLID	BREAKDOWN LASER POWER	ABSORBED LASER POWER	PLASMA TEMPERATURE	PLASMA ELECTRON DENSITY	PROPAGATING VELOCITY	PLASMA LENGTH	PLASMA RADIUS	REFERENCES
CO_2, PULSED 10.6 μm	AIR @ 1 atm	1.06×10^5 W/cm^2	0.53	16000 K	NA	20 cm/sec	0.176 cm	1 cm	REF. 39
CO_2, TEA 10.6 μm	Ar @ 2.9 atm	4×10^5 150 W	290W - 60 kW	20000 K	10^{16}-10^{19} cm^{-3}	NA	0.5 cm	0.5 cm	REF. 40
CO_2, PULSED 10.6 μm	He @ 0.75 atm	NA	0.25 Joule	3×10^4 K	10^{16}-10^{19} cm^{-3}	200 μs* 2×10^5 cm/sec	0.2 cm	0.2 cm	REF. 41
CO_2, 10.6 μm	N_2	NA	50 Joule	750×10^3 K	5×10^{17} cm^{-3}	5×10^7 cm/sec	0.7 cm	BEAM DIA 0.2 cm	REF. 42
RUBY PULSE 1 ns	DEUTERIUM 50 μm	10^{12} W/cm^2	0.08 Joule	125×10^4 K	5×10^{15} cm^{-3}	1.7×10^7 cm/sec	0.01 cm	BEAM DIA 0.01 cm	REF. 43
Nd-GLASS, 25 M W PEAK 40 ns PULSE	AIR @ 1 atm	50 J/cm^2 1.25×10^9 W/cm^2	1 Joule	NA	- 10^{19} cm^{-3}	NA	NA	NA	REF. 44
TVR RUBY 2J/4 ns	DEUTERIUM @ 0.1 0.8 atm	NA	5 ns 135 MW	4.7×10^5 K	1×10^{19} cm^{-3}	4×10^7 cm/sec	0.3 cm	NA	REF. 45
TEA CO_2 0.2J/300 ns	AIR @ 1 atm	2×10^9 W/cm^2	5 J/pulse	NA	NA	2×10^5 cm/sec	0.01 cm	NA	REF. 46
Nd-GLASS (?)	AIR @ 1 atm	2×10^{11} W/cm^2	10 Joule 25 ns	NA	10^{16} - 10^{19} cm^{-3}	2×10^6 cm/sec	4.0 cm	0.7 cm	REF. 47
CO_2 10.6 PULSE	DEUTERIUM & TRITIUM AT VACUUM	NA 10	9×10^2 - 9×10^5 Joule	10 keV	10^{19} cm^{-3}	8.2×10^7 cm/sec	8.2 cm	0.1 cm	REF. 48
CO_2 CW	AIR @ 1 atm	10^5 W/cm^2	2 kW	18000 K	NA	48 cm/sec	1 cm	0.15 cm	REF. 49
CO_2 Q-SWITCHED	Ar @ 2 atm	NA	250 W	21000 K	2.5×10^{17} cm^{-3}	NA	0.2 cm	NA	REF. 50
CO_2, 10.6 μm PULSE	METALS PLASTICS IN AIR	6×10^6 - 4.5×10^7 W/cm^2	20 J 3 MW peak	1.2 4×10^4 K	2.8×10^{18} cm^{-3}	- 3.8×10^5 cm/sec	2.5 cm @ 7 μsec	0.8 cm	REF. 51

*LIFETIME

TABLE V. PARAMETERS NECESSARY FOR CALCULATING THE MHD GENERATOR PERFORMANCE

NO.	PARAMETERS	SYMBOL	CODE	REMARKS
1	TYPE OF GAS			NECESSARY FOR
2	TYPE OF SEED MATERIAL			CALCULATING THE
3	COMPOSITION RATIO, SEED/GAS			STATE VARIABLES
4	AMOUNT OF SEED			AND THE ELECTRICAL
5	GAS DENSITY	N_g		CONDUCTIVITY
6	SEED GAS DENSITY	N_{c_s}		
7	MOLE FRACTION OF SEED	F		
8	INITIAL ELECTRON DENSITY	N_{e_o}		
9	IONIZATION POTENTIAL	V_o		
10	CHARGE OF THE ATOM	Z		
11	TOTAL PRESSURE	P		
12	INITIAL ELECTRON TEMPERATURE	T_{e_o}		
13	DUCT LENGTH	z or ℓ		GEOMETRY
14	DUCT WIDTH	x or W		
15	DUCT HEIGHT	y or L		
16	MAGNET LENGTH	b		
17	DUCT WALL TEMPERATURE	T_w		NECESSARY FOR
18	MAGNETIC FIELD INTENSITY	B		CALCULATING THE
19	FLOW RATE	$\dot{m}$		MHD OUTPUT POWER
20	GENERATOR COEFFICIENT	K		
21	LOAD CURRENT	I		
22	INTERACTION COEFFICENT			

TABLE VI. LASER-PLASMA INTERACTION PARAMETERS USED FOR LASER-DRIVEN MHD

LASER	10.6μ CO_2 PULSED
WORKING FLUID	AIR - 1 atm
BREAKDOWN THRESHOLD LASER POWER	1.3×10^6 W/cm^2
LASER POWER	100 ~ 150 J, 200 ns 10 Hz (EQIUV. CW MODE 50 - 75 MW)
AVERAGE MEDIUM TEMPERATURE IN THE GENERATOR VOLUME	$\geq$ 1600 K
ELECTRON DENSITY	10^{16} ~ 10^{19} cm^{-3}
PROPAGATING VELOCITY	10^6 - 10^7 cm/s
PLASMA LENGTH	15 cm
PLASMA RADIUS	1 cm
SEED MATERIAL	CESIUM

TABLE VII. COMPARISON OF EFFECTS OF TURBULENCE AND NON-EQUILIBRIUM IONIZATION

PARAMETERS	TURBULENCE AND NON-EQUILIBRIUM IONIZATION IGNORED	TURBULENCE AND NON-EQUILIBRIUM IONIZATION TAKEN INTO ACCOUNT
geometry	rectangle cross section	rectangle cross section
n_e, $1/cm^3$	$1.315x10^{19}$	$1.315x10^{19}$
T_e, K	2500	2500 (3100 *)
j, A/cm^2	0.3360	0.3180
K	0.231	0.2843
β	3.17	2.31
P_{out}, W/cm^3	0.225364	0.225364
P_{in}, W/cm^3	**0.420961	0.521918
η, %	53.5	43.2

* The temperature necessary to achieve the efficiency of 53.5%

** Based on T_e, n_e and U, $P_{in} = (n_e \kappa T_e)AU$ per unit volume where A is the cross section area

REFERENCES

1. Colombant, D. G. and W. M. Manheimer: "A Model of Anomalous Absorption, Backscatter, and Flux Limitation in Laser-produced Plasmas," Physics of Fluids, Vol. 21, No. 10, pp. 2512-2528, December 1978.

2. Kruger, C. H. and O. K. Sonju: "On the Turbulent Magnetohydrodynamic Boundary Layer," Proceedings of the 1964 Heat Transfer and Fluid Mechanics Institute, pp. 147-159, Stanford University Press, Stanford, 1964.

3. Harris, L. P.: "Hydromagnetic Channel Flows," MIT Technology Press and John Wiley, 1960.

4. Van Driest: "On Turbulent Flow Near a Wall," Journal of Aeronautical Science, Vol. 23, pp. 1007-1011, 1956.

5. Mei, J. and W. Squire: "A Simple Eddy Viscosity Model for Turbulent Pipe and Channel Flow," AIAA Journal, Vol. 10, pp. 350-352, 1972.

6. Fiveland, W. A.: "An Analytical Stucy of Laminar and Turbulent Mangetofluid Dynamic Boundary Layer Flow with Heat Transfer," Ph.D. Thesis, University of Akron, Ohio, 1978.

7. Voshall, R. E., R. J. Wright and R. W. Lieberman: "Design of Closed-Cycle MHD Generator with Non-equilibrium Ionization and System," IEEE Transactions on Plasma Science, Vol. PS-5, No. 2, June 1977.

8. Zampaglione, V.: "Effective Conductivity of an MHD Plasma in Turbulent State," Electricity from MHD, Vol. 1, International Atomic Energy Agency, Vienna, 1968.

9. Brederlow, G. and K. J. Witte: "Effective Electrical Conductivity and Related Properties of a Non-equilibrium High Pressure MHD Plasma," AIAA Journal, Vol. 12, pp. 83-90, January 1974.

10. Volkov, Y. M.: "Nonisothermal Pulse Discharge in Mixtures of Inert Gasses with Cesium," High Temperature, Vol. 3, pp. 1-11, Jan-Feb, 1965.

11. Kalikham, L. E.: Elements of Magnetohydrodynamics, W. B. Sanders Co., Philadelphia and London, 1967.

12. Shkarofsky, I. P., M. P. Bachynski and T. W. Johnson: "Collision Frequency Associated with High Temperature Air and Scattering Cross-section of the Constituents," RCA Victor Co., Ltd., Report 7-801, December 5, 1959.

13. Lindemuth, I. R., et. al.: "Unstable Behavior of Hot, Magnetized Plasma in Contact with Cold Wall," Physics of Fluids, Vol. 21, No. 10, pp. 1723-1234, October 1978.

14. Holzman, A. L. and J. J. Allport: "Hybrid MHD Pulse Plasma Sources," 8th Symposium on Engineering Aspects of MHD, Stanford, p. 57, March 1967.

15. Louis, J. F.: "Studies on an Inert Gas Disk Hall Generator Driven in a Shock Tunnel," 8th Symposium on Engineering Aspects of MHD, Stanford, p. 75, March 1967.

16. Zauderer, B. and E. Tate: "Experimental Study of the Hall Voltage in a Large Hall Parameter," 8th Symposium on Engineering Aspects of MHD, Stanford, p. 89, March 1967.

17. Chevalley, J. L. and E. Brocher: "A Shockwave MHD Generator using a Nuclear Reactor as an Energy Source," 7th Symposium on Engineering Aspects of MHD, p. 78, March 1966.

18. Sonju, O. K. and J. Teno: "A Two Megawatt High Performance Combustion-Driven MHD Generator Experiment," 12th Symposium on Engineering Aspects of MHD, Argonne, p. II-7.1, March 1972.

19. Dicks, J. B., et. al.: "The Performance of a Family of Diagonal Conducting Wall MHD Open Cycle Generators," 11th Symposium on Engineering Aspects of MHD, Caltec, Pasadena, p. 16, March 1970.

20. Rubin, E. S. and R. H. Eustis: "Electrode Size Effects in Combustion-Driven MHD Generator," 11th Symposium on Engineering Aspects of MHD, Caltec, Pasadena, p. 35, March 1970.

21. Sovie, R. J. and L. D. Nichols: "Results of Initial Subsonic Tests in the NASA-LEWIS Closed-Loop MHD Generator," 11th Symposium on Engineering Aspects of MHD, Caltec, Pasadena, p. 82, March 1970.

22. Roberts, Jr., A. S. and S. Palmgren: "Pulsed MHD Generator Analysis with High Induced Fields," 11th Symposium on Engineering Aspects of MHD, Caltec, Pasadena, p. 135, March 1970.

23. Bohn, T. and P. Komarek: "Experiences and Experimental Results with the Closed-Loop ARGAS I," 10th Symposium on Engineering Aspects of MHD, MIT, Cambridge, p. 172, 1969.

24. Hsu, M. S. S., A. Solbes and J. L. Kerrebrock: "Performance of a Non-Equilibrium MHD Generator with Slanted Electrode Walls," 12th Symposium on Engineering Aspects of MHD, Argonne, p. I-1.1, 1972.

25. Jimerin, D. G., et. al.: "MHD Energy Conversion Using Detonation Conditions," 12th Symposium on Engineering Aspects of MHD, Argonne, p. II-4.1, 1972.

26. Omori, S. and J. Hant: "Cyclone and Fluidized Bed Combustion Concepts for Coal Fired Open Cycle MHD," 17th Symposium on Engineering Aspects of MHD, Stanford, p. A-6.1, 1978.

27. Kirillin, V. A. et. al.: "The U-25B Facility for Studies in Strong MHD Interaction," 17th Symposium on Engineering Aspects of MHD, Stanford, p. F-1.1, 1978.

28. Ramaprasad, V. R.: "Indian Experimental MHD Unit," High Temperature, Vol. 15, No. 5, pp. 911-917, 1977.

29. Palmer, A. J.: "Radiatively Sustained Cesium Plasmas for Solar Electric Conversion," Radiation Energy Conversion in Space, edited by K. W. Billman, Progress in Astronautics and Aeronautics, Vol. 61, AIAA, 1978.

30. Cerini, D. J. and D. G. Elliott: "Performance Characteristics of a Single-Wavelength Liqiud Metal MHD Induction Generator with Endless Compensation," 8th Symposium on Engineering Aspects of MHD, Stanford, p. 11, 1967.

31. Rowe, I., T. C. Wand and S. J. Dudzinsky: "Experimental Results with the Variable Fluid and Field Velocity MHD Generator," 8th Symposium on Engineering Aspects of MHD, Stanford, p. 31, 1967.

32. Amend, M., C. Hsu, M. Petrick and J. Roberts: "Performance of a Quasi-Ericsson Two-Phase Two-Component Liquid Metal MHD Power Cycle," 11th Symposium on Engineering Aspects of MHD, Caltec, Pasadena, p. 154, 1970.

33. Amend, W. E., J. C. Cutting and M. Petrick: "Analysis of Liqiud-Metal MHD Power Cycles for Central Station Power Generation," 12th Symposium on Engineering Aspects of MHD, Argonne, p. N-1.1, 1972.

34. Cerini, D. J.: "Nak-Nitrogen Liquid Metal MHD Generator Tests at 30 KW," 13th Symposium on Engineering Aspects of MHD, Stanford, p. III-2.2, 1973.

35. Hays, L. G., R. L. Phen and P. S. Zygielbaum: "A Cesium-Lithium MHD Topping Plant for Central Station Power Generation," 13th Symposium on Engineering Aspects of MHD, Stanford, p. III-6.1, 1973.

36. Elliott, D. G.: "Performance Capabilities of Liqiud Metal MHD Induction Generators," International Atomic Energy Agency, Proceedings of a Symposium on MHD Electrical Power Generation, Section 2, pp. 1311-2092, July 1968.

37. Petrick, M., P. F. Dunn, E. S. Pierson, P. V. Dauzvardis and I. Pollack: "Liquid Metal MHD Energy Conversion," ANL/MHD-78-5, Argonne National Laboratory, May 1979.

38. Pierson, E. S., H. Branover, G. Fabris and C. B. Reed" "Solor-Powered Liquid Metal MHD Power Systems," ASME, 79-WA/SOL.-22.

39. Batteh, J. H. and D. R. Keefer: "Two Dimensional Generalization of Raizer's Analysis for the Subsonic Propagation of Laser Sparks," IEEE Transactions on Plasma Science, Vol. PS-2, pp. 122-129, September 1974.

40. Frazen, D. L.: "Continuous Laser-Sustained Plasmas," J. Appl. Phys., Vol. 44, No. 4, pp. 1727-1723, April 1973.

41. George, E. V., G. Bekefi and B. Ya'akobi: "Structure of the Plasma Fireball Produced by a CO_2 Laser," The Physics of Fluids, Vol. 14, No. 12, pp. 2708-2713, December 1971.

42. Hoffman, A. L.: "Strong Axial Laser Heating of a Theta-Pinch Plasma," Appl. Phys. Lett., Vol. 23, p. 693, 1974.

43. Jarobe, T. R., W. B. Kunkel and A. F. Lietzake: "Study of Plasma Density Distribution Produced by Irradiating a 50 μ Deuterium Pellet on One Side with a Ruby Laser," The Physics of Fluids, Vol. 19, No. 10, pp. 1501-1506, October 1976.

44. Schwarz, H. J. and H. Hora: Laser Interaction and Related Plasma Phenomena, Vol. 2; The Initial States of Laser-Induced Gas Breakdown, by R. Papoular, Plenum Press, New York, 1972.

45. Schwarz, H. J. and H. Hora: Laser Interaction and Related Plasma Phenomena, Vol. 2; Laser-Produced Gaseous Deuterium Plasmas, by A. H. Guenther and W. K. Pendleton, Plenum Press, New York, 1972.

46. Schwarz, H. J. and H. Hora: Laser Interaction and Related Plasma Phenomena, Vol. 2; Influence of Particles on Laser Induced Air Breakdown, by R. J. Hull, D. E. Lencioni and L. C. Marquet, Plenum Press, New York, 1972.

47. Ready, J. F.: Effects of High-Power Laser Radiation, Academic Press, New York, p. 213, Ch. 5, 1971.

48. Daiver, J. W. and H. M. Thompson: "Laser-Driven Detonation Waves in Gases," Phys. Fluids 10, p. 1162, 1967.

49. Yamanaka, T., N. Tsuchimori, T. Sasaki and C. Yamanaka: "High Density and High Temperature Plasma Produced by Large Power Laser," No. 814, Plasma Production by Laser, 1968.

50. Raizer, Y. P.: "Subsonic Propagation of a Light Spark and Threshold Conditions for the Maintenance of Plasma by Radiation," Soviet Physics JETP, Vol. 31, No. 5, December 1970.

51. Hall, R. B., W. E. Maher and P. S. P. Wei: "An Investigation of Laser-Supported Detonation Waves," AFWL-TR-73-28, June 1973.

52. Meyerand, R. G. and A. F. Haught: "Gas Breakdown at Optical Frequencies," Phys. Rev. Lett., No. 11, p. 401, 1963.

53. Smith, D. C. and A. F. Haught: "Energy Loss Processes in Optical-Frequency Gas Breakdown," No. 16, p. 1085, 1966.

54. Phelps, A. V., et. al.: "Investigation of Gas Ionization Phenomenon at Optical and IR Frequencies," Tech. Rep. No. RADC-TR-65-133, AD 467, p. 392, June 1965.

55. Tomlinson, R. G. and E. K. Damon: "Experimental Data on the Breakdown of Air and Argon by a Ruby Laser Pulse," Ohio State University, Res. Foundation Rep., AD 443, p. 784, June 1964.

56. Buscher, H. T., R. G. Tomlinson and E. K. Damon: "Frequency Dependence of Optically Induced Gas Breakdown," Physics Review Letters, No. 15, p. 847, 1965.

1. Report No.	2. Government Accession No.	3. Recipient's Catalog No.
NASA CR-178184		

4. Title and Subtitle	5. Report Date
Space-Based Laser-Driven MHD Generator: Feasibility Study	October 1986
	6. Performing Organization Code
7. Author(s)	8. Performing Organization Report No.
S. H. Choi	681104
	10. Work Unit No.
9. Performing Organization Name and Address Information & Control Systems, Inc. 28 Research Drive Hampton, VA 23666	11. Contract or Grant No. L-28161B
	13. Type of Report and Period Covered Contractor Report
12. Sponsoring Agency Name and Address National Aeronautics and Space Administration Washington, DC 20546	14. Sponsoring Agency Code 506-41-41-02

15. Supplementary Notes

Langley Technical Monitor: Nelson Jalufka
Final Report

16. Abstract

The feasibility of a laser-driven MHD generator, as a candidate receiver for a space-based laser power transmission system, was investigated.

On the basis of reasonable parameters obtained in the literature search, a model of the laser-driven MHD generator was developed with the assumptions of a steady, turbulent, two-dimensional flow. The assumptions used in this study were based on the continuous and steady generation of plasmas by the exposure of the continuous wave laser beam thus inducing a steady back pressure that enables the medium to flow steadily. The model considered here took the turbulent nature of plasmas into account in the two-dimensional geometry of the generator. For these conditions with the plasma parameters defining the thermal conductivity, viscosity, electrical conductivity for the plasma flow, a generator efficiency of 53.3% was calculated. If turbulent effects and nonequilibrium ionization are taken into account, the efficiency is 43.2%.

An extensive literature search of research on MHD generators and laser-produced plasmas was carried out. The study shows that the laser-driven MHD system has potential as a laser power receiver for space applications because of its high energy conversion efficiency, high energy density and relatively simple mechanism as compared to other energy conversion cycles.

17. Key Words (Suggested by Author(s))	18. Distribution Statement
Space power transmission, lasers, MHD	Unclassified-Unlimited Subject Category 20

19. Security Classif. (of this report)	20. Security Classif. (of this page)	21. No. of Pages	22. Price
Unclassified	Unclassified	51	A04

N-305

For sale by the National Technical Information Service, Springfield, Virginia 22161